

Ubiquitin ligase Nedd4-2 modulates Kv1.3 current amplitude and ion channel protein targeting

Patricio Vélez,^{1*} Austin B. Schwartz,^{2*} Subashini R. Iyer,¹ Anthony Warrington,³
and Debra Ann Fadool^{1,2,3}

¹Program in Neuroscience, Florida State University, Tallahassee, Florida; ²Institute of Molecular Biophysics, Florida State University, Tallahassee, Florida; and ³Department of Biological Sciences, Florida State University, Tallahassee, Florida

Submitted 11 September 2015; accepted in final form 4 May 2016

Vélez P, Schwartz AB, Iyer SR, Warrington A, Fadool DA. Ubiquitin ligase Nedd4-2 modulates Kv1.3 current amplitude and ion channel protein targeting. *J Neurophysiol* 116: 671–685, 2016. First published May 4, 2016; doi:10.1152/jn.00874.2015.—Voltage-dependent potassium channels (Kv) go beyond the stabilization of the resting potential and regulate biochemical pathways, regulate intracellular signaling, and detect energy homeostasis. Because targeted deletion and pharmacological block of the Kv1.3 channel protein produce marked changes in metabolism, resistance to diet-induced obesity, and changes in olfactory structure and function, this investigation explored Nedd4-2-mediated ubiquitination and degradation to regulate Kv1.3 channel density. Heterologous coexpression of Nedd4-2 ligase and Kv1.3 in HEK 293 cells reduced Kv1.3 current density without modulation of kinetic properties as measured by patch-clamp electrophysiology. Modulation of current density was dependent on ligase activity and was lost through point mutation of cysteine 938 in the catalytic site of the ligase (Nedd4-2CS). Incorporation of adaptor protein Grb10 relieved Nedd4-2-induced current suppression as did application of the proteasome inhibitor Mg-132. SDS-PAGE and immunoprecipitation strategies demonstrated a channel/adaptor/ligase signalplex. Pixel immunodensity was reduced for Kv1.3 in the presence of Nedd4-2, which was eliminated upon additional incorporation of Grb10. We confirmed Nedd4-2/Grb10 coimmunoprecipitation and observed an increased immunodensity for Nedd4-2 in the presence of Kv1.3 plus Grb10, regardless of whether the catalytic site was active. Kv1.3/Nedd4-2 were reciprocally coimmunoprecipitated, whereby mutation of the COOH-terminal, SH3-recognition (493–498), or ubiquitination sites on Kv1.3 (lysines 467, 476, 498) retained coimmunoprecipitation, while the latter prevented the reduction in channel density. A model is presented for which an atypical interaction outside the canonical PY motif may permit channel/ligase interaction to lead to protein degradation and reduced current density, which can involve Nedd4-2/Grb10 interactions to disrupt Kv1.3 loss of current density.

potassium channel; olfactory; adaptor protein; ubiquitination; modulation

NEW & NEWSWORTHY

Potassium ion (K) channels are the dampeners of excitation and a novel means of regulating this excitation is through interaction with protein partners that can control channel density at the membrane. An enzyme that tags K channels for degradation is found to interact with discreet

* P. Vélez and A. B. Schwartz contributed equally to this work.

Address for reprint requests and other correspondence: D. A. Fadool, 319 Stadium Drive, Suite 3008, Program in Neuroscience and Molecular Biophysics, Dept. of Biological Sciences, The Florida State Univ., Tallahassee, FL 32306 (e-mail: dfadool@bio.fsu.edu).

residues on the COOH-terminal domain to mediate ubiquitination and functional loss of channel current. The presence of an adaptor protein to the enzyme can reverse this modulation.

THE DEGREE OF EXCITABILITY and the biophysical properties of a neuronal cell membrane depend on the cadre of expressed ion channels; their density and distribution. With regards to voltage-dependent potassium channels (Kv), changes in channel density can have profound effects on the stabilization of the resting potential and repolarization of the action potential (Bean 2007). Cell functions as diverse as neuronal integration, vesicle secretion, or muscle contraction, for example (Korn and Trapani 2005; Zeberg et al. 2010), have the capacity to be modulated via altered electrical properties driven by changes in channel density. The role of Kv channels, therefore, reaches well beyond regulators of excitability and into the realm of regulation of biochemical pathways, intracellular signaling proteins, and a plethora of nonconducting functions (Kaczmarek 2006). Of interest in this investigation is the voltage-gated potassium channel, Kv1.3, a mammalian homolog of the *Shaker* subfamily, which carries a large proportion of the outward voltage-activated current in mitral cell neurons of the olfactory bulb and for which expression drives the interspike interval and intrinsic firing properties of this first order neuron to encode olfactory information (Fadool and Levitan 1998; Fadool et al. 2004, 2011). Not only are these channels important for olfactory discrimination and odor threshold detection (Fadool et al. 2004), deletion of the Kv1.3 gene produces marked changes in metabolism, ingestive behavior, olfactory circuitry development, and glucose sensing (Fadool et al. 2004; Biju et al. 2008; Tucker et al. 2008, 2012a, 2013). Therefore, a protein that typically subserves to dampen the excitability of the nervous system can in tandem be part of a regulatory cascade that permits the olfactory system to detect internal metabolic state to homeostatically counterbalance diet-induced obesity and related metabolic disorders (for review, see Palouzier-Paulignan et al. 2012).

Because mice with a gene-targeted deletion of Kv1.3—/— are thin and do not gain weight when challenged with fatty diets or when bred to models of genetic-linked obesity (Xu et al. 2003; Fadool et al. 2004; Tucker et al. 2008, 2012b), we sought endogenous means to regulate Kv1.3 current density as a future potential means to enhance metabolism. We have previously demonstrated that Kv1.3 is the core of a scaffold of many interacting kinases and adaptor proteins, whose expression and adjacency in olfactory bulb neurons can modulate current density and resident half-life of the channel at the

membrane surface (Holmes et al. 1996; Fadool and Levitan 1998; Fadool et al. 2000; Cook and Fadool 2002; Colley et al. 2007, 2009; Marks and Fadool 2007; Marks et al. 2009). Within the context of this protein-protein signalplex that is well characterized to affect Kv1.3 biophysical properties, we hypothesized that ubiquitination and select degradation of Kv1.3 might be a method of targeted regulation of Kv1.3 density. Potassium channels from the Kv1.x subfamily are targets for Nedd4-2-mediated ubiquitination and degradation primarily using alternative or atypical target recognition motifs or via formation of activation complexes with adaptor proteins or kinases (Henke et al. 2004; Boehmer et al. 2008; Mia et al. 2012; Andersen et al. 2012, 2013).

Ubiquitin is a highly conserved 8.5-kDa polypeptide that functions as a molecular tag for internalization and degradation of membrane proteins. The process requires the sequential activation of three enzymes, the last being an E3 ligase that transfers the ubiquitin to lysine residues of the target protein (Harvey and Kumar 1999; Yang and Kumar 2010; Rotin and Staub 2011). In this study, we focused on Nedd4-2 (neuronal precursor cell-expressed developmentally downregulated protein 4-2) as a 120-kDa highly conserved E3 ligase in eukaryotic cells because it has been demonstrated to regulate membrane availability of a number of ion channels (Rotin and Staub 2011; Lang and Shumilina 2013; Goel et al. 2015). As a HECT (homologous to the E6-AP carboxy terminus) class E3 ligase, Nedd4-2 contains four tryptophan-rich WW domains that bind to different proline-rich regions of a target protein, each with different affinities (Sudol and Hunter 2000; Yang and Kumar 2010). For example, the WWI domain binds the PY motif L/PPxY (Chen and Sudol 1995; Kсанов et al. 2001), whereas the WWII domain binds the PxxP motif (Bedford et al. 1997). The WWIII domain, on the other hand, interacts with Pro and Arg/Lys-rich regions or areas containing Pro, Met, Gly (Bedford et al. 1998), and the WWIV domain binds sequences containing phosphoSer- or phosphoThr-Pro (Sudol and Hunter 2000). Nedd4-2 is typically known to interact with PPxY motifs (Yang and Kumar 2010); however, Kv1.3 contains only a single PxxP motif, PXTPF, at amino acids 493–498 with close adjacency to a Lys amino acid. Following binding of Nedd4-2, ubiquitin is transferred to a locally found Lys. HECT ligases, like Nedd4-2, lack specificity for the Lys that is ubiquitinated and are only limited by spatial constraints between interaction domains of the target protein and the ligase (Mattioli and Sixma 2014). Moreover, Nedd4-2 has been demonstrated to form a complex with Grb10 (growth factor receptor-binding protein 10) (Morrione et al. 1999; Vecchione et al. 2003; Huang and Szebenyi 2010), which we know is enriched in the olfactory bulb, coimmunoprecipitates with Kv1.3, downregulates channel expression, and functionally modulates Kv1.3 phosphorylation and voltage-activated currents (Cook and Fadool 2002; Colley et al. 2009).

Understanding how Kv1.3 channel density could be modulated affords a potential therapeutic means to treat diet-induced obesity or diabetes where Kv1.3 protein abundance could be manipulated to upregulate metabolism, increase glucose uptake, or decrease body weight (Xu et al. 2003; Fadool et al. 2004; Tucker et al. 2013; Upadhyay et al. 2013). This study employs a simple mammalian expression system as a means to elucidate the molecular mechanisms of how the Kv1.3 channel is modulated by ubiquitination by Nedd4-2 and interacting

partners. Modulation of Kv1.3 current density via ubiquitination and subsequent degradation could provide a future novel pharmacological target to treat metabolic dysfunction.

METHODS

Solutions and reagents. All salts and general chemical reagents were purchased from Fisher Scientific (Atlanta, GA) or Sigma Chemical (St. Louis, MO). Bath recording solution contained the following (in mM): 150 KCl, 10 HEPES, 1 EGTA, and 0.5 MgCl₂ (pH 7.4). Patch pipette intracellular solution contained the following (in mM): 30 KCl, 120 NaCl, 2 CaCl₂, and 10 HEPES (pH 7.4). Human embryonic kidney (HEK) 293 culture medium was composed of minimal essential media (MEM; 12360; GIBCO, Life Technologies/Invitrogen, Durham, NC) plus 2% penicillin/streptomycin (15140; GIBCO, Invitrogen) and 10% fetal bovine serum (16000; GIBCO, Invitrogen). Cell lysis buffer contained (in mM): 25 Tris (hydroxymethyl) aminomethane (pH 7.5), 150 NaCl, 150 NaF, 0.5 EDTA, and 1.0% Triton X-100 (pH 8.0). Protease and phosphatase inhibitor (PPI) solution was added to the lysis buffer just before use for a final concentration as follows: 1 μg/ml pepstatin A, 1 μg/ml leupeptin, 2 μg/ml aprotinin, 10 μg/ml phenylmethylsulfonyl fluoride, and 10 mM Na₃VO₄. Homogenization buffer contained the following (in mM): 320 sucrose, 10 Tris, 50 KCl, and 1 EDTA (pH 7.8). Wash buffer contained the following (in mM): 25 Tris base (pH 7.5), 150 NaCl, 150 NaF, 0.5 EDTA, and 0.1% Triton X-100. Phosphate-buffered saline (PBS) contained the following (in mM): 136.9 NaCl, 2.7 KCl, 10.1 Na₂HPO₄, and 1.8 KH₂PO₄ (pH 7.4). The proteasome inhibitor MG-132 was purchased from Calbiochem/EDM Millipore (Billerica, MA) and reconstituted in 0.01% DMSO.

Antisera. FSU120, a rabbit polyclonal antiserum, was generated against the 46-amino acid sequence 478-MVIEEGGMNHSAFPQTPFKTGNSTATCTTNNPNDCVNKIKIFTDV-523, representing the unique coding region of the Kv1.3 channel between transmembrane domain 6 and the carboxy terminal. The purified peptide was produced by Genmed Synthesis (San Francisco, CA) and the antiserum was produced and then affinity purified by Cocalico Biologicals (Reamstown, PA). This antibody was used for immunoprecipitation (1:1,000) and Western blot detection (1:1,500) of Kv1.3 and screened for lack of antigenicity against Kv1.4 and Kv1.5 subfamily members. Anti-c-myc mouse monoclonal (clone 9E10; antigenic peptide EQKLISEEDL directed against the human myc protein) was purchased from Roche (Madison, WI) and used at 1:400 for Western analysis. Anti-Nedd4-2, a rabbit polyclonal antibody generated against the WW domain, was purchased from EDM Millipore and used at 1:2,000 for Western analysis and immunoprecipitation. Grb10 (K-20), a rabbit polyclonal antibody generated by Santa Cruz Biotechnology (Santa Cruz, CA), was used at 1:300 for Western blots and immunoprecipitation. Equivalent protein loading was confirmed using monoclonal anti-actin (Clone C4; Millipore or Clone AC-74; Sigma Chemical) between 1:800 to 1:3,500. Donkey anti-rabbit secondary (1:3000; Amersham/GE Healthcare Life Sciences, Piscataway, NJ) or goat anti-mouse IgG (Fab specific) secondary (1:3000; Sigma Chemical) antisera conjugated to horseradish peroxidase were used to visualize proteins via enhanced chemiluminescence (ECL).

cDNA constructs. All channel and adaptor protein coding regions were downstream from a cytomegalovirus (CMV) promoter. Kv1.3 channel was subcloned into the multiple cloning region of pcDNA3 (Invitrogen) at the unique restriction *HindIII* site as previously described (Holmes et al. 1996). The 10-amino acid c-myc epitope (EQKLISEEDL) was inserted into the extracellular S1/S2 loop between residues 226–227 of Kv1.3 channel via two consecutive polymerase chain reactions (PCRs) using the Expand Long Template PCR System (Roche) as previously described (Colley et al. 2007). Both the untagged channel and the epitope-tagged version of the channel were used in this study as required for surface expression experiments. We have previously demonstrated that the tag does not alter channel

biophysical properties or protein interactions (Colley et al. 2007). Two Kv1.3 COOH-terminal mutants channels were constructed whereby the first was designed to disrupt the PxxP domain as a known SH₃ recognition motif for the WW domain of Nedd4-2 and the second was designed to remove the lysine residues in the COOH terminus that were predicted ubiquitination sites. For the former, prolines (P) 493 and 496 were altered by single-point mutagenesis to glycine (G) (construct called Kv1.ΔSH₃C). For the latter, we used the UbPred (Rockefeller University) to predict strong protein ubiquitination sites based on sequence. There were three sites that had a probability greater than 70% in the COOH terminus (467-70%, 476-91%, and 498-91%) so a triple point site-directed mutagenesis of K to R was performed (construct called KRC Kv1.3). Mutation of K to R is a well-known and common technique to prevent ubiquitination at target Lys (Morén et al. 2003; Tan et al. 2008; Jin et al. 2016). Both Kv1.3 channel mutants were constructed with the use of two sequential PCRs. The first PCR used a mutagenic primer and an upstream primer. The second PCR used the amplified gel-purified product of the first reaction and the downstream oligonucleotide as primers. In this way a stretch of mutant DNA flanked by two unique restriction sites was obtained; the product was double digested and ligated into the parent channel backbone with the use of T4 DNA. All mutant channel constructs were sequenced to verify the mutation and detect PCR errors. Wild-type Nedd4-2 (pCMV-sport6-Nedd4-2) and its inactive form (Nedd-CS; mutation of cysteine to alanine at position 942) were generously donated by Dr. Andrea Morrione (Thomas Jefferson University, Philadelphia, PA) (Vecchione et al. 2003). Nedd4-2 and Nedd-CS were independently sub-cloned into pcDNA3 using *KpnI* and *XbaI* restriction sites. Grb10 cDNA was a gift from Dr. R. Roth (Stanford University, Stanford, CA) in the pECE vector and sub-cloned into pcDNA3 (Colley et al. 2009). Kv1.4 and Kv1.5 cDNA were both expressed in pcDNA3 and were a generous gift from Todd Holmes (University of California Irvine, Irvine, CA) (Nitabach et al. 2002). pCDM8 was a kind gift from Dr. Brian Seed (Harvard University, Boston, MA) (Jurman et al. 1994). DNA encoding human CD8 was amplified from pCDM8 and subcloned into the pcDNA₃ vector between the *BamHI* and *EcoRI* restriction sites (Mast et al. 2010).

Maintenance and transfection of HEK 293 cells. Human embryonic kidney (HEK) 293 cells were maintained in supplemented MEM (See *Solutions and reagents*). Before transient transfection, cells were grown to 100% confluency (7 days), dissociated with trypsin-EDTA (Sigma) and mechanical trituration, diluted in MEM to a concentration of 600 cells/ml, and replated on Corning dishes (catalog no. 25000; Fisher Scientific). cDNA was introduced into HEK 293 cells with a LipofectamineTM transfection reagent in OptiMEM serum-reduced media (Invitrogen/GIBCO) 3–5 days after passage as previously described (Cook and Fadool 2002). Briefly, cells were transfected for 4–5 h (h) with 1.0 μg of each cDNA construct per 35-mm dish for electrophysiology or 3.5 μg of each cDNA construct per 60-mm dish for biochemistry. Plasmid DNA with no coding insert (control vector) served as the control to equalize total μg of cDNA added to each dish. Cells were either harvested for biochemical analysis or used for electrophysiological recordings 30–40 h after transfection.

Protein chemistry. Cells were harvested 2 days posttransfection by lysis in ice-cold lysis plus PPI solution (see *Solutions and reagents*). The lysates were clarified by centrifugation at 14,000 *g* for 10 min at 4°C and then precleared for 1 h with 2–3 mg/ml protein A-Sepharose (Amersham/GE Healthcare Life Sciences), followed by another centrifugation to remove the protein A-Sepharose. The Kv1.3 channel (or protein of interest in parallel experiments) was immunoprecipitated from the cleared lysates by incubation overnight with ~5 μg/ml FSU120 (or specific antibody) at 4°C, followed by a 3-h incubation with protein A-Sepharose and centrifugation as before. The immunoprecipitates were washed four times with ice cold lysate + PPI solution (modified to contain 0.1% Triton X-100). Lysates and

washed immunoprecipitates were diluted in sodium dodecyl sulfate (SDS) gel-loading buffer (Sambrook et al. 1989). Proteins were separated on 8–10% acrylamide gels by SDS-PAGE, followed by electro-transfer to nitrocellulose membranes using 7.5 to 20 μg of protein/lane as determined by a Bradford Assay (Bio-Rad, Hercules, CA). Surface-expressed Kv1.3 proteins (myc epitope tagged) were similarly processed for immunoprecipitation, however, the proteins were alternatively labeled for 30 min at 37°C using 5 μg/ml anti-myc diluted in supplemented MEM before cell lysis. Surface immunoprecipitated channel was therefore not precleared, but was incubated the next day with Protein A-sepharose, centrifuged, washed, and diluted as above. Labeled proteins were visualized using ECL (GE Healthcare Biosciences) exposure on Fugi Rx film (Mid Scientific, St. Louis, MO). Quantitative densitometry of the film autoradiographs was performed using a Hewlett-Packard Scanner (model Scanjet 4850; Hewlett Packard, San Diego, CA) in combination with Quantiscan software (Biosoft, Cambridge, UK). To standardize for any variation in the Western blot transfer or ECL exposure, density ratios for target samples with respect to the channel alone transfection condition (i.e., Kv1.3 + Nedd4-2/Kv1.3) were calculated for proteins from SDS gels which had been electrophoresed together, electro-transferred to the same piece of nitrocellulose, and exposed to the same piece of X-ray film. Nitrocellulose (no. 162-0115, 0.45 μm; Bio-Rad) was either cut or stripped (46430, PLUS stripping reagent; Fisher Scientific) and re-probed with anti-β-actin to standardize differences in loading. Normalized immunodensity values for a given visualized protein were then compared across transfection treatment by using an arcsin transformation for percentage data with a one-way ANOVA at the 95% confidence level ($\alpha \leq 0.05$) with a Student-Newman-Keuls follow-up test (SNK).

Electrophysiology. Thirty-six hours posttransfection, HEK293 cells were rinsed with bath solution and incubated with anti-hCD8 beads (Dyna-Beads; Invitrogen) to mark transfected cells (Jurman et al. 1994; Mast et al. 2010). Coexpression with CD8 allows visualization of cells taking up the cDNA encoding the channel or receptor of interest by marking transfected cells with a red polypropylene-antibody-linked bead. We have demonstrated that single cells take up multiple constructs equivalently and that the density of the beads is proportional to the expression of channel of interest (Cook and Fadool 2002). Cells were rinsed two times with bath solution before beginning a recording session to remove any unbound beads.

Hoffman modulation contrast optics was used to visualize cells at ×40 magnification (Axiovert 135; Carl Zeiss, Thornwood, NY). Patch electrodes were fabricated from Jencons glass (M15/10; Jencons, Bedfordshire, UK) with pipette resistances between 9 and 14 MΩ as fabricated with a vertical puller (PP-830; Narishige, Tokyo, Japan) and fire polished with a microforge (MF-830; Narishige). Macroscopic Kv1.3 currents were recorded at room temperature from cell-attached membrane patches of HEK293 cells using an Axopatch-200B (Molecular Devices/Axon Instruments, Sunnyvale, CA) patch-clamp amplifier. The cell-attached configuration was achieved after carefully contacting the cell surface with the tip of the patch pipette and applying a gentle suction to create a very high resistance (>1 gigaohm) seal. Both the seal and pipette capacitance were electronically compensated before recording. All voltage signals were generated and data were acquired with the use of an Axon Digidata 1200 board with pClamp v10.3 software (Molecular Devices/Axon Instruments). Recordings were filtered at 2 kHz and digitized at 2–5 kHz. Patches were routinely held at a holding potential (V_h) of −90 mV and stepped in 10- to 20-mV depolarizing potentials to +40 mV (V_c) using a pulse duration (P_d) varying from 100 to 1,000 ms. Longer P_d were generally delivered at intervals of 60 s or longer to prevent cumulative inactivation of the Kv1.3 channel (Marom et al. 1993).

Electrophysiological records were analyzed using software from Microcal Origin (Northampton, MA) and Quattro Pro (Borland International, Scotts Valley, CA). Kv1.3 peak current amplitude, channel inactivation (τ_{inact}) and deactivation (τ_{deact}) kinetics, voltage at one-

half maximal activation ($V_{1/2}$), and slope of voltage dependence (κ) were measured in the presence of Nedd4-2 and the presence or absence of the adaptor protein Grb10. Each biophysical property was analyzed in the form of nonnormalized data by Student's t -test at the 95% confidence level to determine any statistical difference in Kv1.3 channel function in the presence of the ligase or adaptor proteins. For comparisons of change in current-voltage relationships in the presence or absence of Nedd4-2 or presence or absence Grb10, a blocked factorial design two-way ANOVA was performed with voltage and transfection condition as factors with a Bonferroni's post hoc comparison to designate significant difference. Fitting parameters for inactivation and deactivation kinetics were as previously described (Cook and Fadool 2002). Briefly, the inactivation of the macroscopic current, during a 1,000-ms voltage step from -90 to $+40$ mV, was fit to the sum of two exponentials by minimizing the sums of squares using a biexponential function [$y = y_0 + A_1e^{-(x-x_0)/\tau_1} + A_2e^{-(x-x_0)/\tau_2}$]. The two inactivation time constants (τ_1 and τ_2) were combined by multiplying each by its weight (A) and summing. The deactivation of the macroscopic current was fit similarly but to a single exponential [$y = y_0 + Ae^{-(x-x_0)/\tau}$]. Tail current amplitudes were plotted in a current-voltage relationship and fit to a Boltzmann sigmoidal curve ($Y = \{(A_1 + A_2)/[1 + e^{(x-x_0)/dx}] + A_2\}$) to calculate the slope of voltage dependence (κ) and voltage at half-activation ($V_{1/2}$) for Kv1.3. To study cumulative inactivation of Kv1.3

under the control condition and in the presence of Nedd4-2 and/or Grb10 adaptor protein, patches were held at -90 mV and stepped to $+40$ mV 12 times using a similar pulse duration as above but recording using different interpulse intervals, including 60, 30, 10, 2, 1, and 0.5 s. Peak current amplitudes were normalized to the initial trace in each series for a given interpulse interval. Cumulative inactivation was always present with interpulse intervals <60 s in the control (Kv1.3 alone) transfection condition, and as much as 50% of channels were caught in the inactivated state with repeated stimulation <2 s.

RESULTS

Ubiquitin ligase Nedd4-2 decreases Kv1.3 current density. To determine whether coexpression of Nedd4-2 with Kv1.3 may functionally downregulate channel density in human cell lines, we transiently cotransfected the channel and ligase in HEK293 cells to record any change in current amplitude in macroscopic cell-attached patches. As demonstrated in Fig. 1A, cotransfection of the ligase produced a decrease in peak current amplitude as exemplified by applying a family of depolarizing voltage steps in 10-mV increments for a patch containing channel alone (Kv1.3) compared with one containing channel

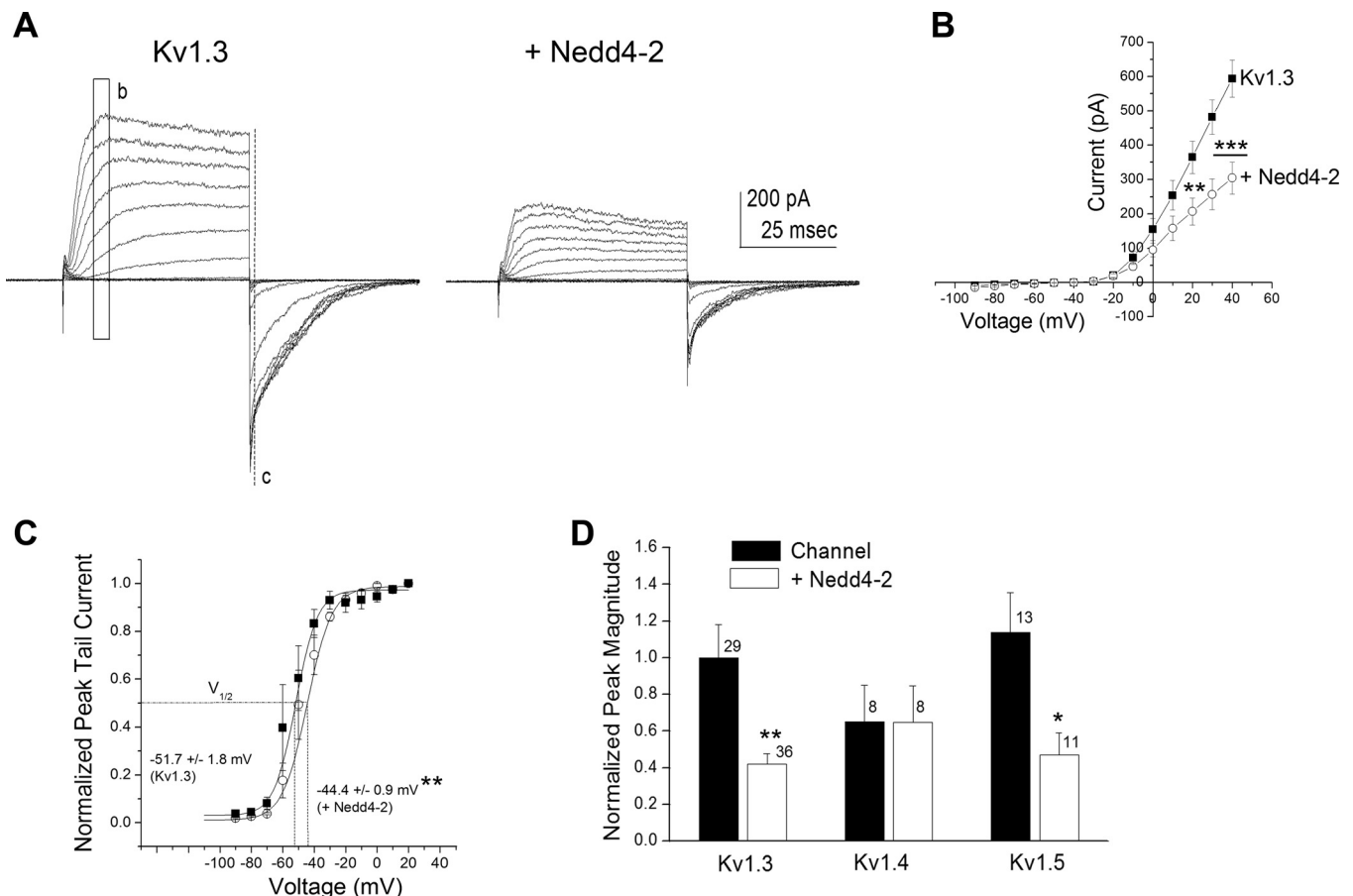


Fig. 1. Nedd4-2 ubiquitin ligase decreases Kv1.3 current amplitude in human embryonic kidney (HEK) 293 cells. *A*: representative cell-attached patch recordings for a HEK 293 cell transfected with Kv1.3 alone (Kv1.3) compared with a cell transfected with Kv1.3 plus Nedd4-2 (+Nedd4-2). Patches were held at -90 mV (V_h) and stepped in 10-mV depolarizing steps (V_c) until reaching $+40$ mV using a pulse duration (P_d) of 100 ms. *B*: mean (\pm SE) current-voltage (I - V) relationship for 5 representative patches recorded as shown in *A* using maximum current amplitude mapped in the region *b*. ■, Kv1.3; ○, + Nedd4-2. ** $P \leq 0.01$, *** $P \leq 0.001$, two-way, mixed repeated measures ANOVA with Bonferroni's post hoc test. *C*: mean (\pm SE) I - V relationship for 5 representative patches recorded as shown in *A* using maximum tail current amplitude mapped in the region *c* to determine voltage at half-activation ($V_{1/2}$). Plot is fit with a Boltzmann relation. ** $P \leq 0.01$, significantly different $V_{1/2}$, Student's t -test. *D*: bar graph of the mean peak current amplitude (mean \pm SE) for a number of recorded patches as in *A* as noted. Values are normalized to that of the Kv1.3 alone transfected condition. Solid bar, channel; open bar, plus ligase. * $P \leq 0.05$, ** $P \leq 0.01$, Student's t -test within *Shaker* subfamily member.

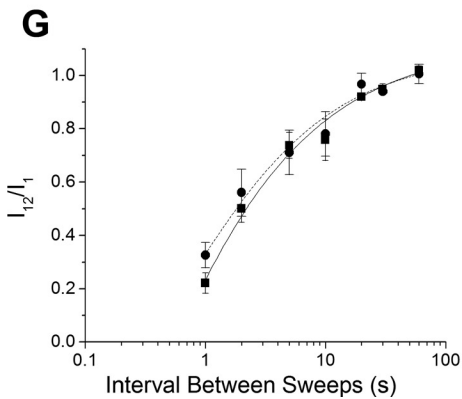
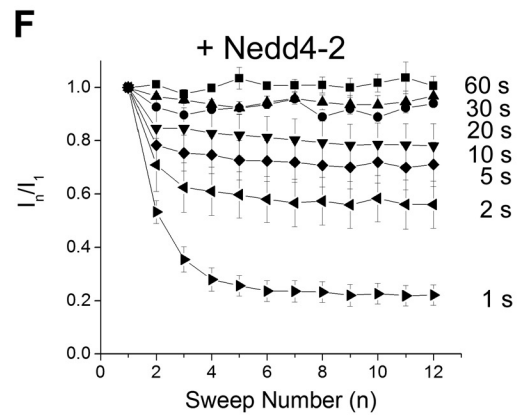
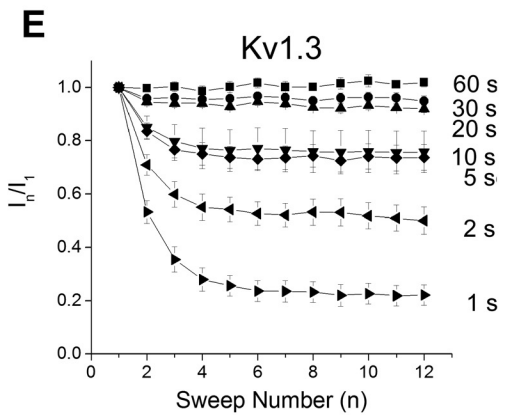
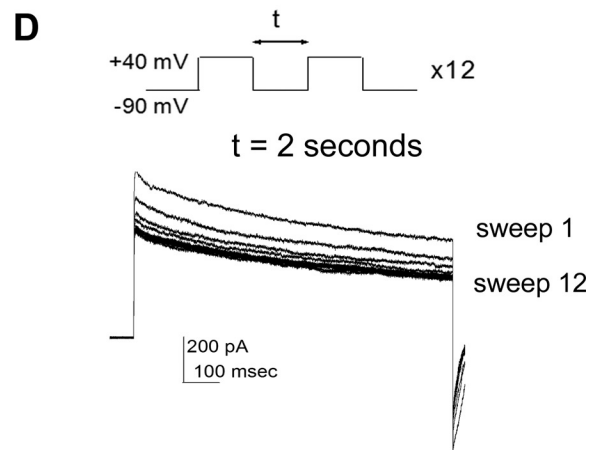
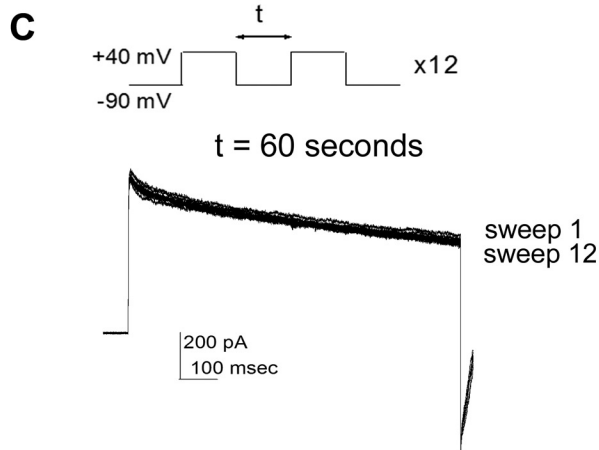
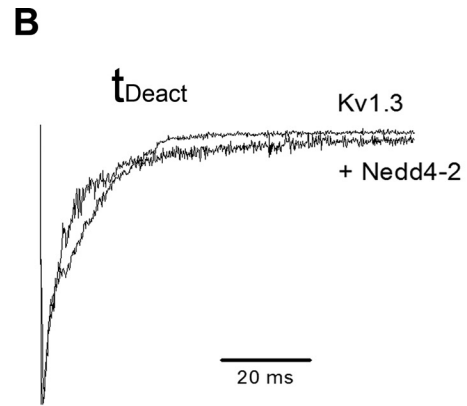
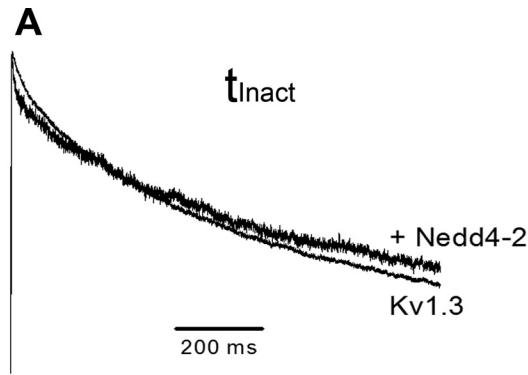
plus ligase (+Nedd4-2). Inclusion of the ligase significantly reduced the peak current amplitude at depolarizing potentials [Fig. 1B; two-way mixed repeated ANOVA with transfection condition and voltage as factors, $F(1,104) = 6.09$, $P \leq 0.05$, $n = 5$]. While the degree of voltage dependence was not altered in the presence of the ligase ($\kappa = 5.35 \pm 0.19$ mV for Kv1.3 vs. 5.26 ± 0.29 mV for +Nedd4-2, Student's t -test, $P \geq 0.05$, $n = 10$), the voltage at half-activation was right shifted ($V_{1/2} = -51.7 \pm 1.8$ mV for Kv1.3 vs. -44.4 ± 0.9 mV for +Nedd4-2, Student's t -test, $P = 0.0067$, $n = 5$; Fig. 1C). Interestingly, in comparing other *Shaker* subfamily members that expressed the LPxY/PPxY motif (Yang and Kumar 2010) recognized by Nedd4-2 (Kv1.5) with those that did not (Kv1.4), Nedd4-2 significantly decreased the peak current amplitude for conditions incorporating the Kv1.3 or Kv1.5 channel but had no effect on those incorporating the Kv1.4 channel (Fig. 1D; significantly different by Student's t -test, $\alpha \leq 0.05$ within channel construct; Kv1.3 $P = 0.0016$; Kv1.4 $P = 0.983$, Kv1.5 $P = 0.0186$). The voltage at half-activation was not significantly different for either Kv1.4 or Kv1.5, albeit only the latter having a PY motif ($V_{1/2} = -42.8 \pm 1.1$ mV for Kv1.4 vs. -40.7 ± 0.4 mV for +Nedd4-2, $n = 4-6$ patches; $V_{1/2} = -31.7 \pm 0.3$ mV for Kv1.5 vs. -29.1 ± 1.1 mV for +Nedd4-2, $n = 9-10$ patches; not significantly different means, Student's t -tests, $P \geq 0.05$).

Ubiquitin ligase Nedd4-2 does not modulate kinetics of Kv1.3. Because channel kinetic properties can contribute to changes in macroscopic current amplitude, we tested whether cotransfection of the ligase was additionally modulating the kinetics of inactivation or deactivation of Kv1.3. Patches were held at -90 mV (V_h) and stepped to a single depolarization ($V_c = +40$ mV) for a P_d of 1,000 ms to allow proper kinetic analysis. There was no significant change in either the τ_{inact} or τ_{deact} for Kv1.3 in the presence of Nedd4-2 ($\tau_{\text{inact}} = 740 \pm 65$ ms for Kv1.3 vs. 723 ± 81 ms for Kv1.3 + Nedd4-2; $\tau_{\text{deact}} = 1.6 \pm 0.9$ ms for Kv1.3 vs. 1.8 ± 0.9 ms for Kv1.3 + Nedd4-2, Student's t -test, $P \geq 0.05$, $n = 20$ to 30 patches), which can also be visibly compared through normalization of the inactivating or deactivating portions of the recorded currents (Fig. 2, A and B). Additionally Kv1.3 exhibits cumulative inactivation with repetitive voltage-activation (Marom et al. 1993; Cook and Fadool 2002); however, unlike with phosphorylation-dependent Kv1.3 modulation (Cook and Fadool 2002), we did not measure any modulation attributable to a change in cumulative inactivation kinetics in the presence of Nedd4-2 (Fig. 2, C–F). Here, patches were held at -90 mV (V_h) and stepped to a $V_c = +40$ mV for 12 sweeps (n) using a P_d of 1000 ms while varying the interpulse interval between sweeps (t) (Fig. 2, C and D). Currents at each sweep (I_n) were normalized to that observed at the first sweep (I_1), or I_n/I_1 , to compare the fraction of the Kv1.3 channels that were caught in the inactivated state following voltage restimulation (t). The fraction of channels not inactivated using a $t = 5-10$ s fell to $\sim 75\%$ for both Kv1.3 and Kv1.3 + Nedd4-2 containing patches and dropped to 50–60% for both transfection conditions using a $t = 2$ s (Fig. 2, E and F). A semi-log plot of t vs. I_2/I_1 demonstrated no effect of the presence of Nedd4-2 on the point at which (t) half the channels were in their inactivated state when fit with a logistic sigmoidal relation (Student's t -test, $P = 0.9937$). These data inferred that the biophysical changes in Kv1.3

protein were likely attributable to changes in channel density or degradation of Kv1.3 from the membrane surface.

Kv1.3 channel density is dependent on ligase activity. We tested whether the active site of Nedd4-2 was required for Kv1.3 current modulation by substituting Nedd4-2CS (C938S Nedd4-2), in which the catalytic site of the ligase is destroyed by point mutation of a cysteine residue (Henke et al. 2004). Under these conditions, cotransfection of Kv1.3 plus Nedd4-2CS failed to decrease current amplitude of the channel (Fig. 3). Because kinetic and voltage dependence changes were not observed in the presence of wild-type Nedd4-2 (Fig. 2) and changes in voltage-activation were modest (Fig. 1C), only current magnitude was further examined. Inclusion of the mutant ligase significantly failed to reduce the peak current amplitude at depolarizing potentials as was observed with the wild-type Nedd4-2 ligase [Fig. 3B; two-way mixed repeated ANOVA with transfection condition and voltage as factors, $F(1,689) = 8.791$, $P \geq 0.05$]. Similarly, when comparing current amplitude at $+40$ mV, the addition of mutant ligase was not significantly different than that of Kv1.3 alone [Fig. 3C, one-way ANOVA with transfection condition as the factor, $F(2,53) = 9.166$, $P \geq 0.05$]. Moreover it was possible to block the modulation of Kv1.3 by wild-type Nedd4-2 if we preincubated cotransfected HEK293 cells with the proteasome inhibitor Mg-132. Here, cotransfected cells were treated with 0, 4, or 8 μM Mg-132 for 12 h before electrophysiological measurements. Representative single step, voltage-activated currents are demonstrated in Fig. 4A. There was significant relief in the suppression of Kv1.3 current by Nedd4-2 following proteasome inhibitor treatment that was dose dependent; at 8 μM Mg-132, patches of the Kv1.3 plus Nedd4-2 cotransfection condition exhibited a peak current magnitude that was not significantly different than that of the Kv1.3 alone condition [Fig. 4B; one-way ANOVA, SNK, $F(3, 78) = 5.159$, $P \geq 0.05$]. Because the solvent for Mg-132 was 0.1% DMSO, a subsample of Kv1.3 plus Nedd4-2 cotransfected cells were also treated with DMSO using the same 12-h preincubation, but this treatment did not modify peak current magnitude compared with control bath treated cells (Student's t -test, $n = 7$, $P = 0.7694$). These data indicate that interaction of Nedd4-2-ubiquitinated Kv1.3 must interact with the multicatalytic protease to initiate degradation of the channel linked to decreased functional density and subsequent current downregulation.

The adaptor protein Grb10 may deregulate ubiquitination of Kv1.3. Because we have previously reported Grb10 interference of kinase-induced modulation of Kv1.3 (Cook and Fadool 2002) and others have reported a Grb10/Nedd4 complex that may form a bridge between Nedd4 and tyrosine kinases (Vecchione et al. 2003), we wondered whether this adaptor protein might modulate the functional interaction between the channel and the ligase. We tested a transfection scheme in which Grb10 plus Nedd4-2 + Kv1.3 was compared with Nedd4-2 + Kv1.3 alone. The addition of Grb10 adaptor protein decreased the ligase-induced suppression of Kv1.3 current (Fig. 5A). Addition of Grb10 to the Kv1.3 + Nedd4-2 cotransfection condition exhibited an I - V relation that was not significantly different than that of Kv1.3 alone [Fig. 5B, two-way mixed design repeated ANOVA, Bonferroni's post hoc test, $F(2, 767) = 14.88$, $P \geq 0.05$]. When comparing current amplitude at $+40$ mV, the addition of Grb10 plus Nedd4-2 was not significantly different than that of Kv1.3 alone [Fig. 5C, one-way ANOVA



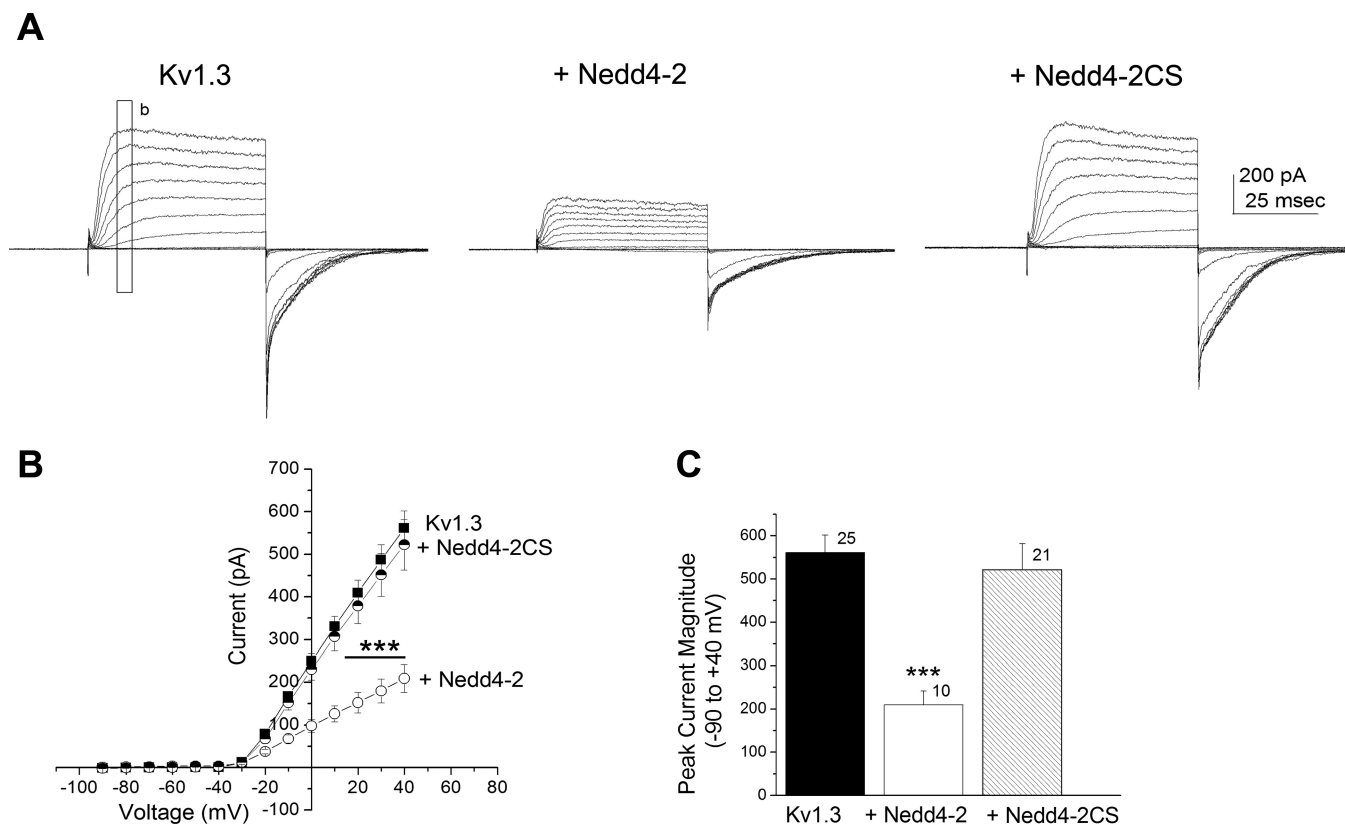


Fig. 3. Mutation of the catalytic site of Nedd4-2 (Nedd4-2CS) renders the ligase ineffective in modulating Kv1.3 current amplitude. *A* and *B*: same voltage paradigm, *I*-*V* plot, and statistical design as in Fig. 1, *A* and *B*, except substitution of a Nedd4-2 ligase with a cysteine to serine point mutation (^{C938S}Nedd4-2) known to disrupt all catalytic activity of the ligase. ■, Kv1.3; ○, + Nedd4-2; half-filled circle, +Nedd4-2CS. *C*: bar graph of the mean (±SE) current amplitude for the -90- to +40-mV step for a number of patches as noted. Solid bar, channel (Kv1.3); open bar, channel plus wild-type ligase (+Nedd4-2); hatched bar, channel plus mutant ligase (+Nedd4-2CS). ****P* ≤ 0.001, one-way ANOVA, Student-Newman-Keuls (SNK) post hoc test.

with transfection condition as the factor, $F(2,59) = 14.42$, $P \geq 0.05$]. We reasoned that the increased current density of the channel under these conditions could be attributed to the reported SH2 domain of Grb10 binding to the C2 domain of Nedd4-2 (Vecchione et al. 2003) that would lessen its ability to ubiquitinate Kv1.3, or Grb10 interaction with Kv1.3 (Cook and Fadool 2002; Colley et al. 2009) could interfere with Nedd4-2 ubiquitination of Kv1.3. In either instance, it was important to determine biochemically the ability of the ligase to ubiquitinate its target. We therefore decided to probe protein-protein interactions of the potential signaling partners involved and confirm degree of potential ubiquitination of Kv1.3 with the availability of specific protein partners.

Protein-protein interactions in a channel/adaptor/ligase signalplex. We generated a Kv1.3 specific antisera as previously designed (called FSU-120) (Tucker and Fadool 2002) and optimized its working dilution range for Kv1.3-transfected HEK 293 cells by Western blot analysis (Fig. 6A). Using both this antisera as well as an epitope-tagged strategy whereby an

extracellular myc sequence was inserted between the S1 and S2 transmembrane domain (Colley et al. 2009), we probed the expression of Kv1.3 channel and found that it decreased in the presence of Nedd4-2 or Grb10 (Fig. 6, *B-D*). The Kv1.3 channel could be immunoprecipitated using anti-myc, separated by SDS-PAGE, and then probed with FSU-120 (Fig. 6*B*) to visual a decrease in channel pixel density in the presence of Nedd4-2 (M vs. MN). When Nedd4-2 plus Grb was cotransfected with the channel, however, the channel pixel density was comparable to that of channel alone (M vs. MNG). As we reported previously, we observed a decrease in Kv1.3 expression when cotransfected with Grb10 alone (Colley et al. 2009), which was further decreased if coexpressed with Nedd4-2 lacking the catalytic site of the ligase (Nedd4-2CS; D, Dead Nedd4-2) (Fig. 6*B*). When we further explored whole cell lysates for the expression of Kv1.3 channel in the presence of wild-type vs. catalytically inactive Nedd4-2, Kv1.3 expression was significantly less in the presence of wild-type Nedd4-2 (M vs. MN). This reduction was slightly relieved when the Nedd4-

Fig. 2. Nedd4-2 ligase does not affect kinetic properties of Kv1.3 ion channel. *A* and *B*: recorded cell patches held at $V_h = -90$ mV and stepping to a single step depolarization (V_c) using a P_d of 1000 ms. Traces are normalized to the peak current amplitude or peak tail current to better visualize the rate of the kinetics of inactivation (*A*) or deactivation (*B*), respectively. Representative of $n = 20-30$ such recordings. *C* and *D*: recorded cell patches using the voltage paradigm in *A* and then modifying the interpulse interval, t , as indicated. Example traces were taken from cells transfected with Kv1.3 alone. *E*: line graph of the mean (±SE) current for cell-attached patches recorded after applying the voltage paradigm in *C* and varying t as noted for 5 to 8 Kv1.3 transfected cells (Kv1.3). Data are normalized to the peak current amplitude at pulse number (n) over that of the initial amplitude for a given t (I_n/I_1). *F*: same as *E*, but for Kv1.3 + Nedd4-2 transfected cells (+Nedd4-2). *G*: log graph of the mean (±SE) I_2/I_1 for 5 patches fit with a logistic sigmoidal relation. ●, Kv1.3 alone; ■, Kv1.3 + Nedd4-2. $P \geq 0.05$, not significantly different inactivation τ at half-max, Student's *t*-test.

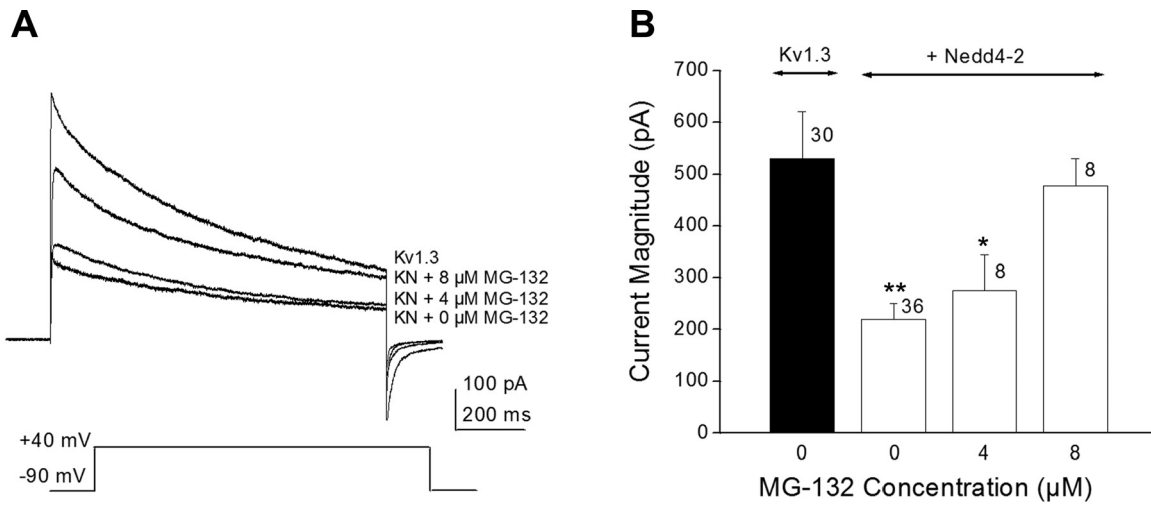


Fig. 4. The protease inhibitor Mg-132 disrupts Nedd4-2-induced Kv1.3 current suppression. *A*: representative voltage-activated currents elicited from three different HEK 293 cells cotransfected with Kv1.3 plus Nedd4-2 and which had been preincubated for 12 h with various concentrations of Mg-132. $V_h = -90$ mV, $V_c = +40$ mV, $P_d = 1000$ ms, $t = 60$ s. The 0 Mg-132 condition applied the concentration of DMSO used as a solvent for the other inhibitor treated patches. A Kv1.3 alone trace (without ligase and without inhibitor) is shown as a comparison. *B*: bar graph of the mean voltage-activated currents (mean \pm SE) for a number of patches recorded with noted inhibitor concentrations. * $P \leq 0.05$, ** $P \leq 0.01$, one-way ANOVA with SNK post hoc test; $n =$ number of patches.

2CS was substituted for wild-type Nedd4-2; however, the pixel immunodensity of the channel remained significantly less than that of Kv1.3 transfection condition alone [Fig. 6C-D, one-way ANOVA, SNK, $F(5,33) = 12$, $P \leq 0.0001$]. Interestingly, Nedd4-2 expression appeared to be increased when Grb10

adaptor was coexpressed with the channel, regardless of whether the ligase was catalytically active or not [Fig. 7, A and B, one-way ANOVA, SNK, $F(4,18) = 4.71$, $P = 0.016$]. As has been previously reported by others (Vecchione et al. 2003; Huang and Szebenyi 2010), we were able to reciprocally

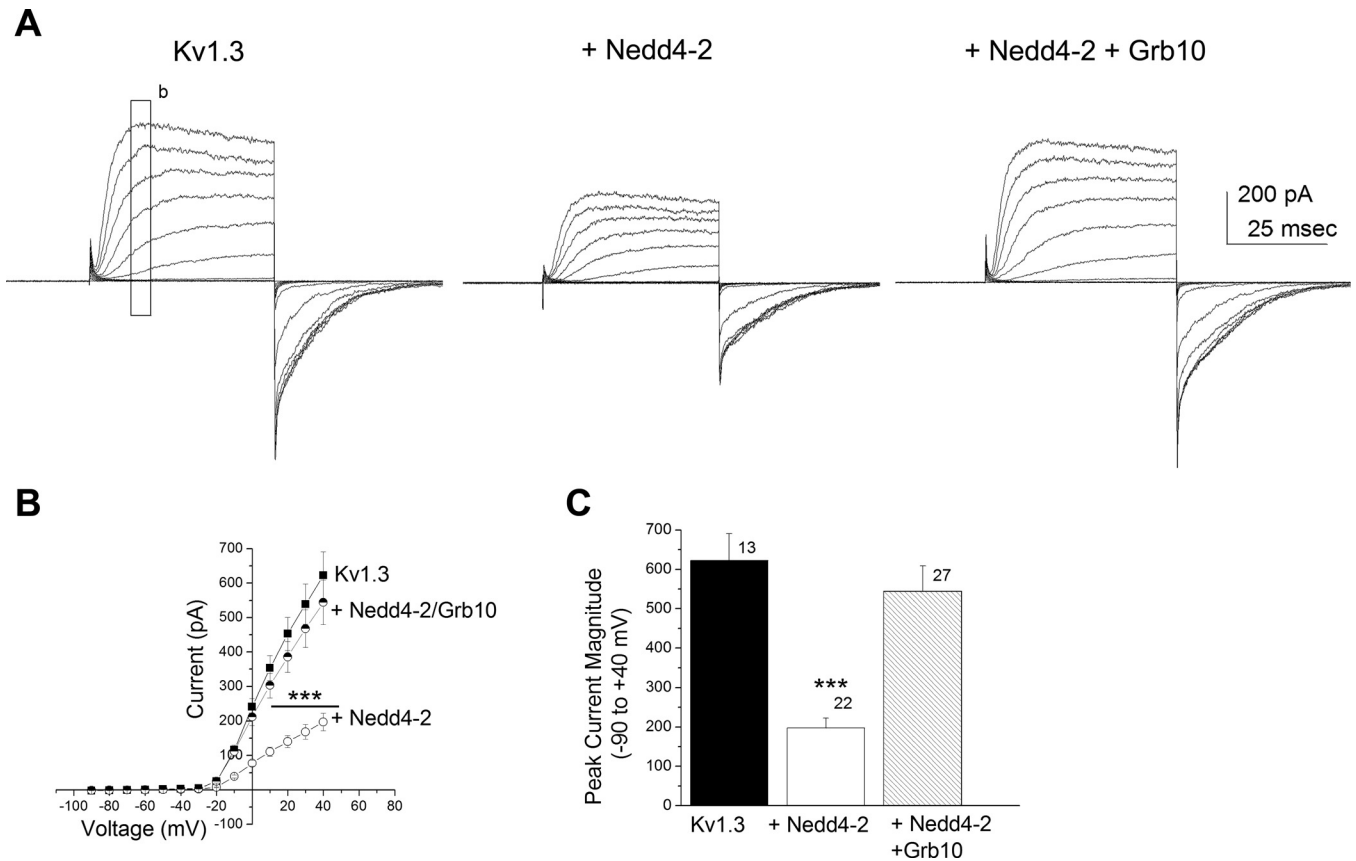


Fig. 5. Adaptor protein Grb10 decreases Nedd4-2-induced Kv1.3 current suppression. *A-C*: same voltage paradigm, *I-V* plot, bar graph plot, and statistical designs as in Fig. 3, except comparing Nedd4-2 alone (+Nedd4-2) vs. Nedd4-2 plus Grb10 (+Nedd4-2 + Grb10) modulation of Kv1.3 current (Kv1.3). Solid bar, channel (Kv1.3); open bar, channel plus ligase (+Nedd4-2); hatched bar, channel, ligase, and adaptor protein (+Nedd4-2 + Grb10). *** $P \leq 0.001$, one-way ANOVA, Student-Newman-Keuls (SNK) post hoc test.

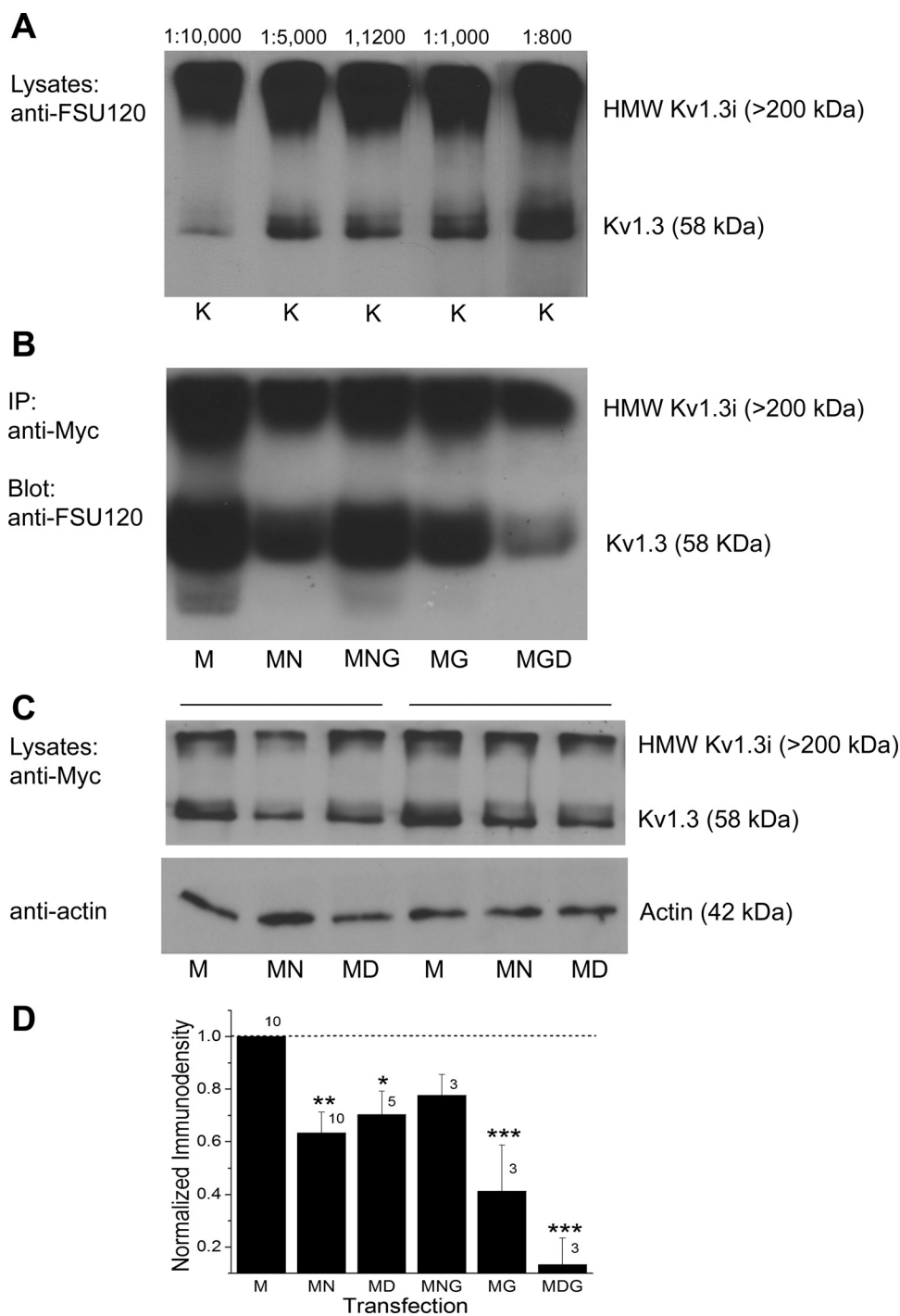
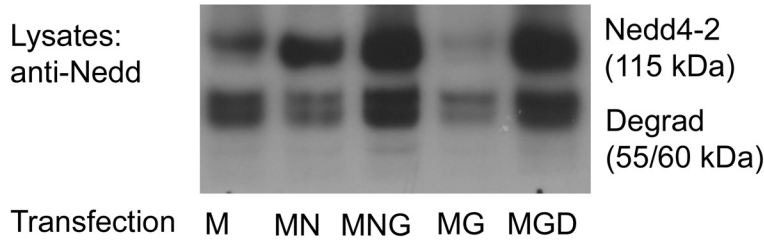


Fig. 6. Coexpression of Nedd4-2 with Kv1.3 causes a decreased expression of the channel, which can be relieved with the addition of Grb10 adapter protein. *A*, Western blot of a homogeneous front of cell lysates (Lysates) prepared from HEK 293 cells transfected with Kv1.3 channel (K). Proteins were separated by 10% SDS-PAGE and electrotransferred to nitrocellulose. Nitrocellulose blots were probed with antiserum generated against the Kv1.3 COOH terminus (see text, anti-FSU120) at the noted dilutions ranging from 1:800 to 1:10,000. $M_r = 58$ kDa for the Kv1.3 channel (Kv1.3), also visible are the high molecular weight multimers of the 4 channel subunits (HMW Kv1.3i, > 200 kDa). *B*: same separation strategy as in *A*, but where individually transfected samples are first immunoprecipitated (IP) with anti-myc (1:400), separated by SDS-PAGE, and then blotted with anti-FSU-120 (1:1,000). *C*: same separation strategy as in *A*, but lysates are probed for anti-myc (1:400) or anti-actin (1:800). Bars above Western blot indicate repeated transfection plan of 2 different trial sets. M, Myc-tagged Kv1.3 channel; N = Nedd4-2; G, Grb10; D, dead Nedd4-2 (Nedd4-2CS). *D*: bar graph of the normalized immunodensity values of the collective protein bands and correlate sample size for the noted transfection conditions. * $P \leq 0.05$, ** $P \leq 0.01$, *** $P \leq 0.001$, one-way ANOVA with SNK post hoc test; n = number of transfection samples. Dashed line, immunodensity value for Kv1.3 transfected condition alone.

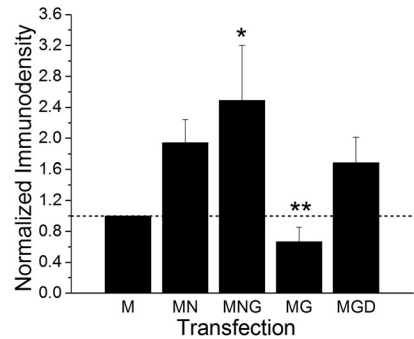
coimmunoprecipitate Nedd4-2 and Grb10 adaptor protein and did not observe a significant reduction in this association when all three constructs were cotransfected and the ligase catalytic site was inactive [KNG vs. KDG; Fig. 7C, D, one-way ANOVA, $F(7,23) = 0.85$, $P = 0.56$]. It was possible to

reciprocally coimmunoprecipitate the channel and Nedd4-2, indicating there was a protein-protein interaction between the channel and the ligase (Fig. 7E, F). This interaction appeared to be enhanced in the presence of Grb10 adaptor when the channel was immunoprecipitated and then probed for ligase

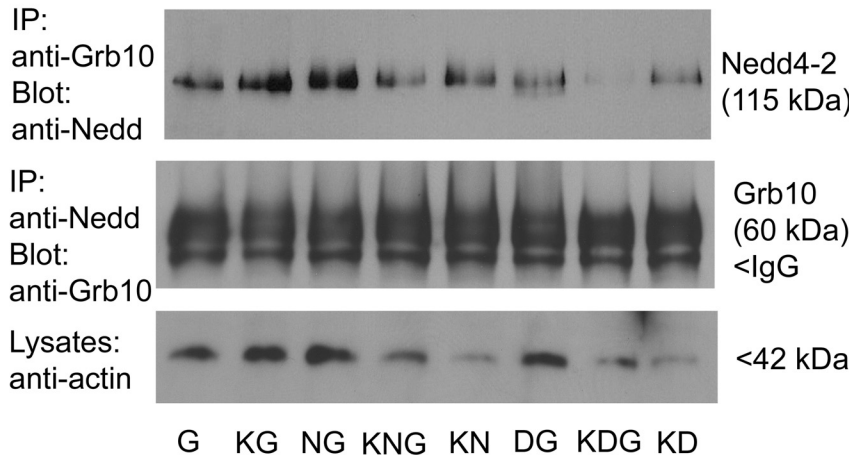
A



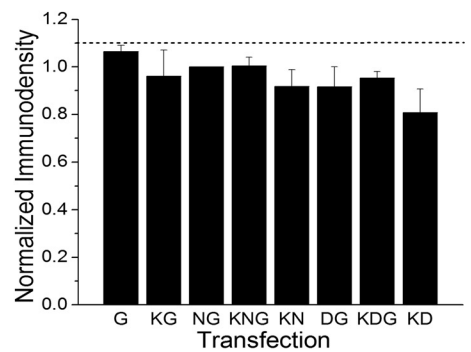
B



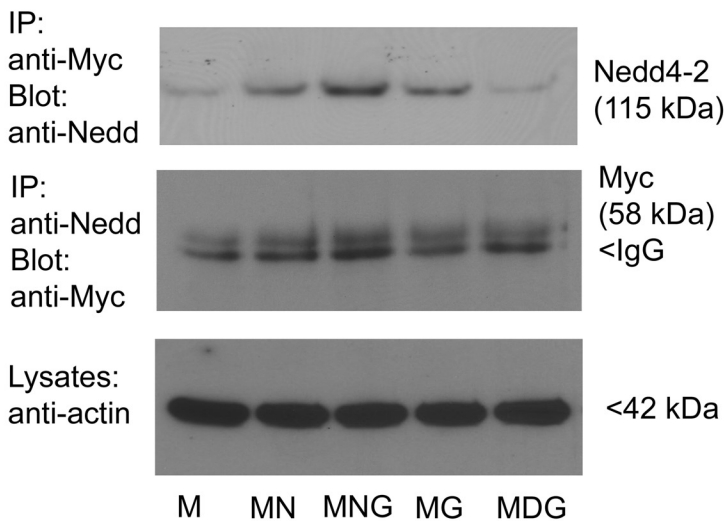
C



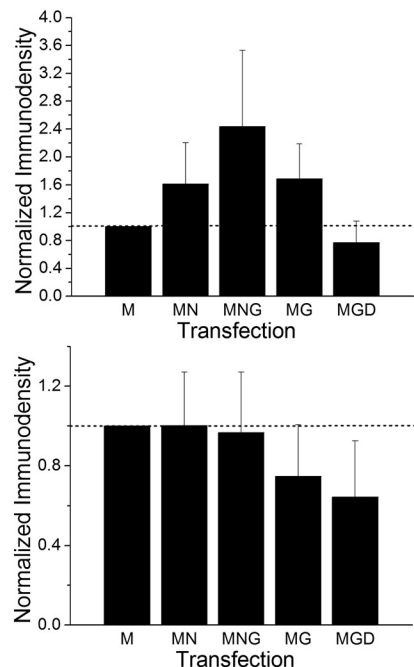
D



E



F



interaction. This signalplex was dependent on activity of the catalytic site of Nedd4-2, but this did not reach statistical significance [MNG vs. MDG; Fig. 7, *E* and *F*; IP myc, blot Nedd: one-way ANOVA, $F(4,14) = 2.0$, $P = 0.18$; IP Nedd, blot myc: one-way ANOVA, $F(4,19) = 1.204$, $P = 0.35$]. An endogenous low expression of ligase and adaptor protein was observed in the HEK293 cells that was apparent under transfection conditions lacking Nedd4-2 or Grb10 (Fig. 7, *A–E*). Therefore, Kv1.3/Nedd4-2 can form a signaling complex regardless of the presence of Grb; however, the strength of the association trended to vary with the presence of Grb or the catalytic activity of the ligase.

The proline-rich motif, 493PQTPF498, is not required for channel-ligase interaction or functional modulation. We had previously identified that the PxxPx sequence at 493–498 functionally perturbed postsynaptic density 95 (PSD-95) modulation of insulin-induced Kv1.3 current suppression (Marks and Fadool 2007) even though it was not required for PSD-95/Kv1.3 protein-protein interaction. Given that this same motif can serve as a binding site for Nedd4-2 and could correspond well with the spatial constraints of the COOH-terminal lysines (Mattiroli and Sixma 2014), we examined whether Kv1.ΔSH₃C and Nedd4-2 could be coimmunoprecipitated (Fig. 8, *A* and *B*). We were able to reciprocally coimmunoprecipitate the Kv1.ΔSH₃C and the ligase, indicating that the PxxPx sequence was not required for channel/ligase interaction [not significantly different pixel densities, one-way ANOVA, SNK, $F(5,23) = 0.69$, $P = 0.64$]. Destruction of the proline-rich SH₃ recognition motif in the channel also did not interfere with the ability of Nedd4-2 to decrease Kv1.3 channel density [Fig. 8*C*, one-way ANOVA with transfection condition as the factor, Bonferroni's post hoc test, $F(2, 75) = 6.86$, $P \leq 0.0019$]. The combination of the biochemical and electrophysiological results infer that there must be a noncanonical site for channel/ligase interaction that does not involve this SH₃ recognition motif.

Lysines 467, 476, and 498 are potential targets of Kv1.3 ubiquitination. Despite lack of experimental evidence for PxxPx at Kv1.3 residues 493–498 to allow protein-protein interaction between the channel/ligase via Nedd4-2 WW domain, the strongest prediction of protein ubiquitination site using the UbPred (Rockefeller University) still resided adjacent to this site at three lysines in the COOH-terminal, with a probability greater than 70% of being ubiquitinated (467-70%, 476-91%, and 498-91%). We therefore cotransfected our generated triple-point mutant channel (KRC Kv1.3) with Nedd4-2 to determine if removal of all three putative lysine residues in proximity to the proline-rich, COOH-terminal region (Fig. 9) would disrupt Nedd4-2 modulation of Kv1.3 current. As dem-

onstrated in Fig. 8*D*, cotransfection of Nedd4-2 plus KRC Kv1.3 no longer decreased peak current amplitude (not significantly different, paired *t*-test, $P \geq 0.05$), indicating that this lysine cluster was essential for ubiquitination. Change in the ability of Nedd4-2 to decrease current density of KRC Kv1.3 did not affect protein-protein interaction of the ligase and the channel. KRC Kv1.3/Nedd4-2 could be reciprocally coimmunoprecipitated as shown in Fig. 8, *A* and *B*, despite its lack of ability to be modulated (Fig. 8*D*). The combination of these biochemical and electrophysiological results infers that strong interaction in the COOH-terminal SH₃ recognition motif was not necessary for lysine-targeted functional modulation.

DISCUSSION

We have demonstrated that it is possible to downregulate Kv1.3 channel density through activation of an E3 ubiquitin ligase and that inhibition of the protease pathway or mutation of the Nedd4-2 catalytic site prevents Kv1.3 modulation. The fact that an additional endogenous pathway for regulating Kv1.3 current has been uncovered may allow a unique mechanism to fine tune olfactory discrimination and the detection of metabolic cues at the level of the olfactory bulb.

Nedd4-2 modulation of Kv1.3 occurs by ubiquitination of the protein in preparation for its degradation by lysosomes so that it cannot contribute to membrane excitability. Because the design of our experiments used a cotransfection scheme, we do not know the time course of modulation by Nedd4-2; however, there are some interesting comparisons to other channel modulators. Kv1.3 is a substrate or target for multiple signaling proteins that modulate its biophysics in a time and metabolic state-dependent manner (Tucker and Fadool 2002; Marks et al. 2009; Fadool et al. 2011). While several kinases are known to phosphorylate the channel, phosphorylation does not appear to degrade Kv1.3 but rather decreases current amplitude through a conformational change, likely attributable to the addition of the phosphate moiety. In fact, the decreased current amplitude can be slowly reversed within the duration of a patch-clamp recording through application of kinase inhibitors (Fadool and Levitan 1998), so it is unlikely that modulation by phosphorylation is due to protein degradation. Other sources of Kv1.3 modulation are too rapid for protein degradation, occurring within minutes and completely reversible upon application of a wash, such as found with glucose or glucagon-like peptide (Tucker et al. 2013; Thiebaud et al. 2016). Modulation by Nedd4-2 additionally only alters current amplitude, consistent with a degradative process, unlike that found with phosphorylation or attributable to auxiliary subunits, which are known to affect kinetic processes (Bowlby et al. 1997; Cook and Fadool 2002; Pongs and Schwarz 2010).

Fig. 7. Grb10 adaptor protein enhances expression of Nedd4-2; Nedd4-2 forms a protein-protein interaction with Grb10 and with Kv1.3. *A*: protein separation strategy, Western blot, and transfection abbreviations as in Fig. 6. Nitrocellulose blots were probed with antiserum directed against Nedd4-2 (anti-Nedd, 1:2,000 dilution), $M_r = 115$ kDa. Note the increased expression of Nedd4-2 in the presence of Grb10 regardless of whether the catalytic site of the ligase was present or not (MNG vs. MGD). Note also a lower, doublet degradation product at 55/60 kDa, recognized by the manufacturer of the antibody. *B*: bar graph of the normalized immunodensity values of the collective protein bands for 4 experiments performed as in *A*; transfection conditions as noted. $*P \leq 0.05$, $**P \leq 0.01$, one-way ANOVA with SNK post hoc test. Dashed line, immunodensity value for Kv1.3 transfected condition alone. *C*: prepared lysates were either immunoprecipitated (IP) with Grb10 antibody (IP: anti-Grb10) and then blotted with Nedd4-2 (Blot: anti-Nedd, 1:2000), $M_r = 115$ kDa; or the reciprocal (IP: anti-Nedd/Blot: anti-Grb10, 1:800), $M_r = 60$ kDa. Input was also probed with anti-actin (1:800). *D*: bar graph of the normalized immunodensity values for three experiments performed for IP: anti-Nedd/Blot: anti-Grb10 as in *C*; notation and statistical analysis as above, not significantly different, $P \geq 0.05$. *E*: prepared lysates were immunoprecipitated with myc antibody (IP: anti-Myc) and then blotted with Nedd4-2 (Blot: anti-Nedd, 1:2000), $M_r = 115$ kDa; or the reciprocal (IP: anti-Nedd/Blot: anti-Myc, 1:400), $M_r = 58$ kDa. Input was also probed with anti-actin (1:800). *F*: bar graph of the normalized immunodensity values for three experiments performed for each type of IP shown in *E*. Notation and statistical analyses as above, not significantly different, $P \geq 0.05$.

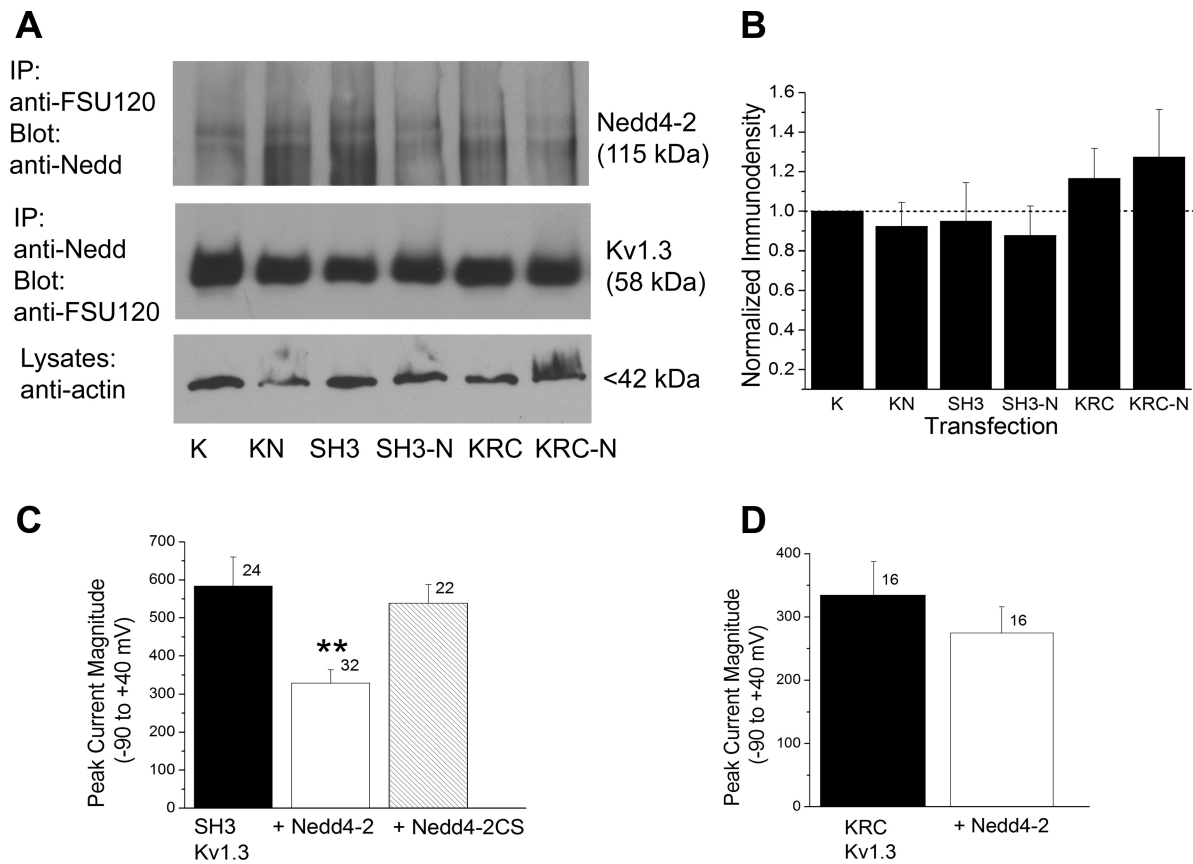


Fig. 8. Nedd4-2 and Kv1.3 form a protein-protein interaction that is not dependent on the SH₃ recognition motif, PQTPF even though destruction of neighboring ubiquitination targets (K) causes a loss of Nedd4-2-evoked decrease in channel density. *A*: prepared lysates were either immunoprecipitated (IP) with Kv1.3 antibody (IP: anti-FSU-120) and then blotted with Nedd4-2 (Blot: anti-Nedd, 1:2,000), $M_r = 115$ kDa; or the reciprocal (IP: anti-Nedd/Blot: anti-FSU-120, 1:1,000), $M_r = 58$ kDa. Input was also probed with anti-actin (1:800). K, Kv1.3; KN, Kv1.3 plus Nedd4-2; SH3, Kv1.3 plus Nedd4-2; SH3-N, Kv1.3 plus Nedd4-2; KRC, triple point channel mutation of K to R at residues 467, 476, 498; KRC-N, triple point channel mutation plus Nedd4-2. *B*: bar graph of the normalized immunodensity values of the collective protein bands for four experiments performed for IP: anti-Nedd/Blot: anti-FSU-120 as in *A*; notations and statistical analysis as in Fig. 7, not significantly different, $P \geq 0.05$. *C*: bar graph of the mean (\pm SE) current amplitude recorded for patches stepped from -90 to $+40$ mV as in Fig. 3C but substituting Kv1.3 channel lacking the COOH terminal PY recognition motif. Solid bar, Kv1.3 Δ SH₃C; open bar, Kv1.3 Δ SH₃C plus wild-type ligase (+Nedd4-2); hatched bar, Kv1.3 Δ SH₃C plus mutant ligase (+Nedd4-2CS). ** $P \leq 0.01$, one-way ANOVA, SNK post hoc test. *D*: bar graph as in *C*, but substituting Kv1.3 channel lacking the 3 K residues at 467, 476, and 498. Solid bar, KRC Kv1.3; open bar, KRC Kv1.3 plus ligase (+Nedd4-2). $P \geq 0.05$, Student's *t*-test.

Nedd4-2 has been demonstrated to regulate the membrane availability of a number of ion channels (Bongiorno et al. 2011). This includes a variety of voltage-dependent ion channels such as Na 1.1, 1.2, 1.3, 1.5, 1.6, 1.7, and 1.8 that contain the typical PY motif (Fotia et al. 2004; Rougier et al. 2005) and voltage-dependent chloride channels like ClC-2 and ClC-5 that display alternative recognition sequences (Palmada et al. 2004; Rickheit et al. 2010). Structurally, Nedd4-2 contains an NH₂-terminal Ca-dependent membrane translocation domain (C2 domain) and a COOH-terminal catalytic domain named HECT domain (Fig. 9). This domain binds specific E2 enzymes, accepts ubiquitin from E2 to form an ubiquitin-thioester intermediate with the HECT active cysteine (C703 in human Nedd4-2), and then transfers ubiquitin to either the ϵ -amino groups of lysine side chains of the substrate or to the growing end of multiubiquitin chains (Huang et al. 1999). Between C2 and HECT domains, Nedd4-2 contains three or four tryptophan-rich domains (WW domains) important for protein-protein interaction and target recognition via the proline-rich (PY) motifs of the substrate protein (Lu et al. 1999) (Fig. 9). Kv1.3 does not have the typical PPxY motif; therefore, another site may be involved that would permit protein-protein interactions

of the channel and the ligase as observed in our reciprocal coimmunoprecipitation experiments. The accessible PQTPF motif (493–498) in the COOH-terminal domain of Kv1.3 was the most suspected target for interaction due to the adjacency of three K amino acids that could subserve the ubiquitination function. Because our mutagenesis data indicate that Kv1.3 Δ SH₃C and Nedd4-2 can coimmunoprecipitate without any functional disruption of Nedd4-2-induced reduction in Kv1.3 channel density, this SH₃ recognition motif is not necessary for association to allow channel downregulation. This suggests that Kv1.3 utilizes an atypical or alternative binding motif for interaction (Lu et al. 1999; Ingham et al. 2004; Persaud et al. 2009; Yang and Kumar 2010). This would not be unexpected given that several Kv7.x family members have been found to be regulated by Nedd4-2 via the channel COOH-terminus (Jespersen et al. 2007). Kato et al. (2005) have shown that inhibition of the proteasome complex increases Kv1.5 current secondary to channel protein stabilization. Henke et al. (2004) and Boehmer et al. (2008) report Nedd4-2-induced ubiquitination of Kv1.3 and Kv1.5 respectively, demonstrating a down regulation of current density as expressed in *Xenopus* oocytes, but neither group mutagenized the suspected interac-

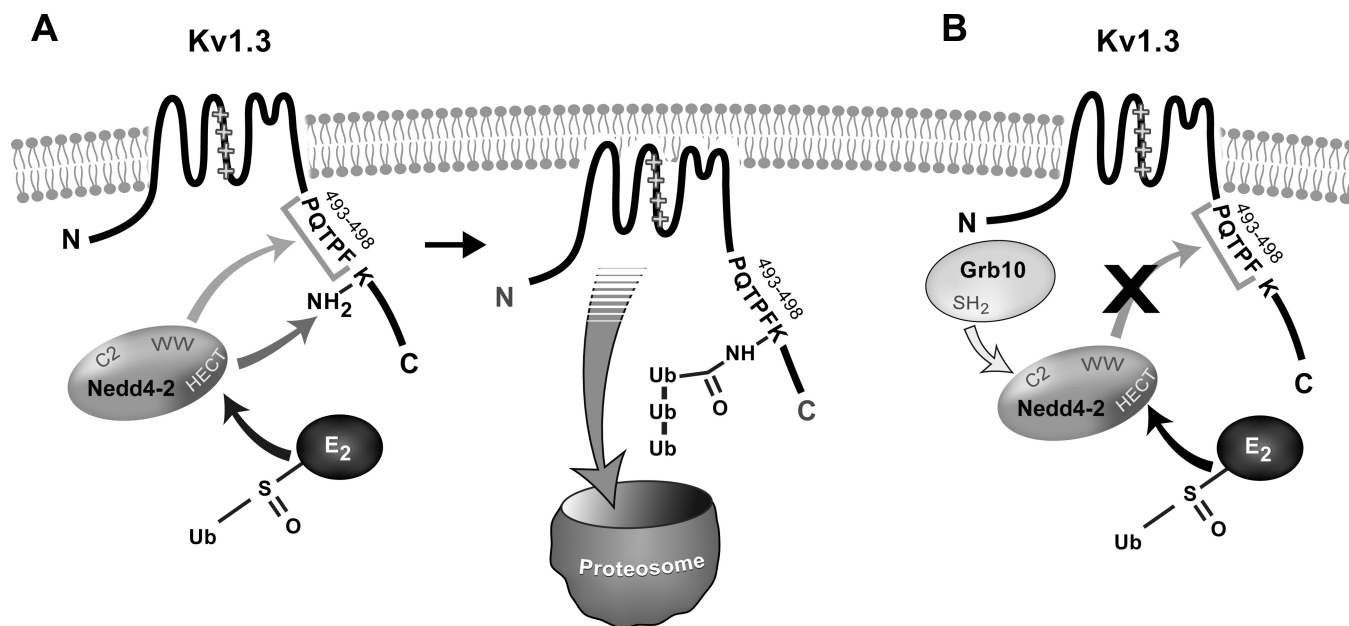


Fig. 9. Schematic of Kv1.3, Nedd4-2, and Grb10 interactions. We propose a model by which Nedd4-2 can either *A*, interact with Kv1.3 channel to initiate degradation and decrease channel density, or *B*, interact with Grb10 adaptor protein (Grb10) to prevent Kv1.3 loss of function. Nedd4-2 contains an NH₂-terminal Ca-dependent membrane translocation domain (C2 domain), a COOH-terminal catalytic domain named HECT domain (homologous to the E6-AP carboxy terminus), and tryptophan-rich domains (WW). In *A*, the E2 ubiquitin ligase (E2) transfers ubiquitin (Ub) to Nedd4-2 by binding to the HECT domain. The WW domain would be predicted to interact with Kv1.3 at the atypical, proline-rich PY motif, PQTPF, or a nearby alternative motif (arrow) that would allow transfer of ubiquitin to one of the nearby lysine targets (K; 467, 476, 498). Once tagged with ubiquitin, Kv1.3 is pulled out of the cell membrane and trafficked to the proteasome for degradation, thereby resulting in a loss of current and channel density. Our data demonstrate that mutation of the proline-rich PY motif does not interfere with Kv1.3/Nedd4-2 protein-protein interaction, inferring Nedd4-2 binding must be retained at an alternative location that still permits access to the K residues for transfer of ubiquitin. Mutation of the K targets prevents the reduction of Kv1.3 current and channel density by Nedd4-2. In *B*, the SH₂ domain of Grb10 could bind the C2 domain of Nedd4-2, thereby preventing the WW domain of Nedd4-2 from interacting with Kv1.3 and tagging the channel for degradation. With this protein-protein interaction between ligase and adaptor, the channel has no loss of current or channel density.

tion site or target K. Interestingly, sequence comparison between Kv1.3 and Kv1.5 demonstrates that Kv1.5 has two repeats of proline-rich binding motifs between 65 and 73 and 76 and 82 in the NH₂ terminus that reflect high confidence of ubiquitination using the UbPred Software (47–90% and 52–86%). Given the fact that we and others (Boehmer et al. 2008) do not observe a shift in the voltage at half-activation ($V_{1/2}$) for Kv1.5 (Steidl and Yool 1999) in the presence of Nedd4-2 but we record a significant right shift in $V_{1/2}$ for Kv1.3, this would be consistent with a Kv1.3/ligase interaction in the COOH terminus that is closer to the pore and voltage sensor as opposed to a Kv1.5/ligase interaction occurring in the NH₂-terminal region far removed from channel domains regulating conductance. Previous work by Holmes et al. (1996) has also demonstrated protein-protein interactions for Kv1.5 involving these same N terminal, proline-rich binding motifs as recognition motifs for SH₃ domain-containing proteins that are not recognized as interaction motifs in Kv1.3.

In addition to the Nedd4.2/Kv1.3 interaction, Grb10 adaptor is expressed in brain regions of high Kv1.3 protein expression (Colley et al. 2009) and the three could serve as a signalplex. Huang and Szebenyi (2010) recently reported the structural basis of how Grb10 forms a complex with Nedd4-2. It is possible in our study that Grb10 might form a protein complex with Nedd4-2 that then renders Nedd4-2 ineffective to bind and carry out ubiquitination of Kv1.3 (Fig. 9). This model of interaction would be consistent with Nedd4-2 ability to decrease Kv1.3 current (and channel density) and its failure to do so in the presence of Grb10. Due to the endogenous expression of both ligase and adaptor protein in the HEK293 cell lines, our

current studies cannot exclude that Nedd4-2 may use Grb10 as an adaptor to scaffold to the Kv1.3 channel; however, we do not anticipate this to be the case because we have previously failed to coimmunoprecipitate Grb10 and Kv1.3 (Colley et al. 2009).

Select degradation of Kv1.3 may afford a mechanistically distinct method of regulating its involvement in metabolic sensing or balancing of energy homeostasis. It is possible to intranasally deliver Kv1.3 neuromodulators *in vivo* to determine their ability to change physiological processes by targeting Kv1.3 channels in the olfactory bulb (Marks et al. 2009). While some of this work is still in progress, there are some interesting comparisons that are coming to light as to whether these delivered exogenous modulators have the capacity to phenocopy the Kv1.3-targeted deletion in terms of increased metabolism or enhanced olfactory ability. A single administration of intranasal insulin causes robust phosphorylation of Kv1.3 and can change known protein-protein interactions with well-characterized adaptor proteins such as PSD-95 (Marks et al. 2009). More chronic administration of intranasal insulin modestly enhances olfactory discrimination, increases object memory recognition, does not modify reversal learning, and fails to significantly change body weight or total mass specific metabolism (Bell and Fadool, 2015 AChemS Abstract). Alternatively, pilot studies in which the scaffold of Kv1.3 proteins is not manipulated but rather delivery of peptide blockers of the vestibule of Kv1.3 is targeted cause enhanced mass specific metabolism within a few days of delivery to the olfactory bulb using osmotic minipumps (Tucker and Fadool, 2010 AChemS Abstract). It would be interesting to intranasally deliver

Nedd4-2 ligase as a means of degrading Kv1.3 channel and associated protein partners in vivo to determine if removal of the potassium channel protein could phenocopy the thin, obesity-resistant mouse observed in the Kv1.3-targeted deletion (Xu et al. 2003; Fadool et al. 2004; Tucker et al. 2012a,b; Thiebaud et al. 2014). Moreover, because Kv1.3 channel blockers have been systemically demonstrated to decrease body weight, prevent fatty liver disease, and prevent adipose deposition in diet-induced obese models (Upadhyay et al. 2013), having a targeted means of degrading channel protein through ubiquitination may afford a global route of balancing energy homeostasis outside the signaling complex operational in the olfactory bulb.

ACKNOWLEDGMENTS

We thank Cheryl Pye and Brian Washburn in the Florida State University Molecular Cloning Facility for construction of the myc-epitope tagged Kv1.3 construct before our resynthesis of the new Kv1.3 antiserum and assistance with construction of the triple point K channel (KRC Kv1.3). We thank Charles Badland for artistic assistance to display channel/ligase/adaptor interactions in Fig. 9. We also thank Christopher Kovach and Stephanie Zych for technical assistance supporting our experiments.

Present address of P. Véllez: Escuela de Medicina, Universidad de Tarapacá, Arica, Chile.

GRANTS

This work was supported by National Institute on Deafness and Other Communication Disorders Grants R01-DC-003387, R01-DC-013080, and F31-DC-010097. A. Schwartz was supported by the University Legacy Fellowship from Florida State University.

DISCLOSURES

No conflicts of interest, financial or otherwise, are declared by the author(s).

AUTHOR CONTRIBUTIONS

P.V., A.B.S., S.I., A.W., and D.A.F. performed experiments; P.V., A.B.S., and D.A.F. analyzed data; P.V., A.B.S., S.I., A.W., and D.A.F. edited and revised manuscript; P.V., A.B.S., S.I., A.W., and D.A.F. approved final version of manuscript; A.B.S. and D.A.F. interpreted results of experiments; D.A.F. conception and design of research; D.A.F. prepared figures; D.A.F. drafted manuscript.

REFERENCES

- Andersen MN, Krzystanek K, Jespersen T, Olesen SP, Rasmussen HB. AMP-activated protein kinase downregulates Kv7.1 cell surface expression. *Traffic* 13: 143–156, 2012.
- Andersen MN, Krzystanek K, Petersen F, Bomholtz SH, Olesen SP, Abriel H, Jespersen T, Rasmussen HB. A phosphoinositide 3-kinase (PI3K)-serum- and glucocorticoid-inducible kinase 1 (SGK1) pathway promotes Kv7.1 channel surface expression by inhibiting Nedd4-2 protein. *J Biol Chem* 288: 36841–36854, 2013.
- Bean BP. The action potential in mammalian central neurons. *Nat Rev Neurosci* 8: 451–465, 2007.
- Bedford MT, Chan DC, Leder P. WW domains and the Abl SH3 domain bind to a specific class of proline-rich ligands. *EMBO J* 16: 2376–2383, 1997.
- Bedford MT, Reed R, Leder P. WW domain-mediated interactions reveal a spliceosome-associated protein that binds a third class of proline-rich motif: the proline glycine and methionine-rich motif. *Proc Natl Acad Sci USA* 95: 10602–10607, 1998.
- Bell GA, Fadool DA. Behavioral analysis of the effect of acute versus chronic intranasal insulin treatment (Abstract). *Chem Senses* 40: 537, 2015.
- Biju KC, Marks DR, Mast TG, Fadool DA. Deletion of voltage-gated channel affects glomerular refinement and odorant receptor expression in the mouse olfactory system. *J Comp Neurol* 506: 161–179, 2008.
- Boehmer C, Laufer J, Jeyaraj S, Klaus F, Lindner R, Lang F, Palmada M. Modulation of the voltage-gated potassium channel Kv1.5 by the SGK1 protein kinase involves inhibition of channel ubiquitination. *Cell Physiol Biochem* 22: 591–600, 2008.
- Bongiorno D, Schuetz F, Poronnik P, Adams DJ. Regulation of voltage-gated ion channels in excitable cells by the ubiquitin ligases Nedd4 and Nedd4-2. *Channels* 5: 79–88, 2011.
- Bowlby MR, Fadool DA, Levitan IB. Modulation of the Kv1.3 potassium channel by receptor tyrosine kinases. *J Gen Physiol* 110: 601–610, 1997.
- Chen H, Sudol M. The WW domain of Yes-associated protein binds a proline-rich ligand that differs from the consensus established for Src homology 3-binding modules. *Proc Natl Acad Sci USA* 92: 7819–7823, 1995.
- Colley BS, Biju KC, Visegrady A, Campbell S, Fadool DA. Neurotrophin B receptor kinase increases Kv subfamily member 1.3 (Kv13) ion channel half-life and surface expression. *Neuroscience* 144: 531–546, 2007.
- Colley BS, Cavallin MA, Biju K, Marks DR, Fadool DA. Brain-derived neurotrophic factor modulation of Kv1.3 channel is disregulated by adaptor proteins Grb10 and nShc. *BMC Neurosci* 10: 8, 2009.
- Cook KK, Fadool DA. Two adaptor proteins differentially modulate the phosphorylation and biophysics of Kv1.3 ion channel by SRC kinase. *J Biol Chem* 277: 13268–13280, 2002.
- Fadool DA, Levitan IB. Modulation of olfactory bulb neuron potassium current by tyrosine phosphorylation. *J Neurosci* 18: 6126–6137, 1998.
- Fadool DA, Tucker K, Pedarzani P. Mitral cells of the olfactory bulb perform metabolic sensing and are disrupted by obesity at the level of the Kv1.3 ion channel. *PLoS One* 6: e24921, 2011.
- Fadool DA, Tucker K, Perkins R, Fasciani G, Thompson RN, Parsons AD, Overton JM, Koni PA, Flavell RA, Kaczmarek LK. Kv1.3 channel gene-targeted deletion produces “Super-Smeller Mice” with altered glomeruli, interacting scaffolding proteins and biophysics. *Neuron* 41: 389–404, 2004.
- Fadool DA, Tucker K, Phillips JJ, Simmen JA. Brain insulin receptor causes activity-dependent current suppression in the olfactory bulb through multiple phosphorylation of Kv1.3. *J Neurophysiol* 83: 2332–2348, 2000.
- Fotia AB, Ekberg J, Adams DJ, Cook DI, Poronnik P, Kumar S. Regulation of neuronal voltage-gated sodium channels by the ubiquitin-protein ligases Nedd4 and Nedd4-2. *J Biol Chem* 279: 28930–28935, 2004.
- Goel P, Manning JA, Kumar S. NEDD4-2 (NEDD4L): the ubiquitin ligase for multiple membrane proteins. *Gene* 557: 1–10, 2015.
- Harvey KF, Kumar S. Nedd4-like proteins: an emerging family of ubiquitin-protein ligases implicated in diverse cellular functions. *Trends Cell Biol* 9: 166–169, 1999.
- Henke G, Maier G, Wallisch S, Boehmer C, Lang F. Regulation of the voltage gated K⁺ channel Kv1.3 by the ubiquitin ligase Nedd4-2 and the serum and glucocorticoid inducible kinase. SGK1. *J Cell Physiol* 199: 194–199, 2004.
- Holmes TC, Fadool DA, Levitan IB. Tyrosine phosphorylation of the Kv1.3 potassium channel. *J Neurosci* 16: 1581–1590, 1996.
- Holmes TC, Fadool DA, Ren R, Levitan IB. Association of Src tyrosine kinase with a human potassium channel mediated by SH3 domain. *Science* 274: 2089–2091, 1996.
- Huang L, Kinnucan E, Wang G, Beaudenon S, Howley PM, Huijbregtse JM, Pavletich NP. Structure of an E6AP-UbcH7 complex: insights into ubiquitination by the E2–E3 enzyme cascade. *Science* 286: 1321–1326, 1999.
- Huang Q, Szebenyi DM. Structural basis for the interaction between the growth factor-binding protein GRB10 and the E3 ubiquitin ligase NEDD4. *J Biol Chem* 285: 42130–42139, 2010.
- Ingham RJ, Gish G, Pawson T. The Nedd4 family of E3 ubiquitin ligases: functional diversity within a common modular architecture. *Oncogene* 23: 1972–1984, 2004.
- Jespersen T, Membrez M, Nicolas CS, Pitard B, Staub O, Olesen SP, Baró I, Abriel H. The KCNQ1 potassium channel is down-regulated by ubiquitinating enzymes of the Nedd4/Nedd4-like family. *Cardiovasc Res* 74: 64–74, 2007.
- Jin YJ, Cai CY, Zhang X, Burakoff SJ. Lysine 144, a ubiquitin attachment site in HIV-1 Nef, is required for Nef-mediated CD4 down-regulation. *J Immunol* 180: 7878–7886, 2016.
- Jurman ME, Boland LM, Liu Y, Yellen G. Visual identification of individual transfected cells for electrophysiology using antibody-coated beads. *Biotechniques* 17: 876–881, 1994.

- Kaczmarek LK.** Non-conducting functions of voltage-gated ion channels. *Nat Rev Neurosci* 7: 761–771, 2006.
- Kasanov J, Pirozzi G, Uveges AJ, Kay BK.** Characterizing Class I WW domains defines key specificity determinants and generates mutant domains with novel specificities. *Chem Biol* 8: 231–241, 2001.
- Kato M, Ogura K, Miake J, Sasaki N, Taniguchi S, Igawa O, Yoshida A, Hoshikawa Y, Murata M, Nanba E, Kurata Y, Kawata Y, Ninomiya H, Morisaki T, Kitakaze M, Hisatome I.** Evidence for proteasomal degradation of Kv1.5 channel protein. *Biochem Biophys Res Commun* 337: 343–348, 2005.
- Korn SJ, Trapani JG.** Potassium channels. *IEEE Trans Nanobioscience* 4: 21–33, 2005.
- Lang F, Shumilina E.** Regulation of ion channels by the serum- and glucocorticoid-inducible kinase SGK1. *FASEB J* 27: 3–12, 2013.
- Lu PJ, Zhou XZ, Shen M, Lu KP.** Function of WW domains as phosphoserine- or phosphothreonine-binding modules. *Science* 283: 1325–1328, 1999.
- Marks DR, Fadool DA.** Post-synaptic density perturbs insulin-induced Kv1.3 channel modulation via a clustering mechanism involving the SH3 domain. *J Neurochem* 103: 1608–1627, 2007.
- Marks DR, Tucker K, Cavallin MA, Mast TG, Fadool DA.** Awake intranasal insulin delivery modifies protein complexes and alters memory, anxiety, and olfactory behaviors. *J Neurosci* 29: 6734–6751, 2009.
- Marom S, Goldstein SAN, Kupper J, Levitan IB.** Mechanism and modulation of inactivation of the Kv3 potassium channel. *Receptors Channels* 1: 81–88, 1993.
- Mast TG, Brann JH, Fadool DA.** The TRPC2 channel forms protein-protein interactions with Homer and RTP in the rat vomeronasal organ. *BMC Neurosci* 11: 61, 2010.
- Mattioli F, Sixma TK.** Lysine-targeting specificity in ubiquitin and ubiquitin-like modification pathways. *Nat Struct Mol Biol* 21: 308–316, 2014.
- Mia S, Munoz C, Pakladok T, Siraskar G, Voelkl J, SAlesutan I, Lang Downregulation of Kv1 F.5. K channels by the AMP-activated protein kinase. *Cell Physiol Biochem* 30: 1039–1050, 2012.**
- Morén A, Hellman U, Inada Y, Imamura T, Heldin CH, Moustakas A.** Differential ubiquitination defines the functional status of the tumor suppressor Smad4. *J Biol Chem* 278: 33571–33582, 2003.
- Morrione A, Plant P, Valentinis B, Staub O, Kumar S, Rotin D, Basserga R.** mGrb10 interacts with Nedd4. *J Biol Chem* 274: 24094–24099, 1999.
- Nitabach MN, Llamas DA, Thompson IJ, Collins KA, Holmes TC.** Phosphorylation-dependent and phosphorylation-independent modes of modulation of shaker family voltage-gated potassium channels by SRC family protein tyrosine kinases. *J Neurosci* 22: 7913–7922, 2002.
- Palmada M, Dieter M, Speil A, Bohmer C, Mack AF, Wagner HJ, Klingel K, Kandolf R, Murer H, Biber J, Closs EI, Lang F.** Regulation of intestinal phosphate cotransporter NaPi IIb by ubiquitin ligase Nedd4-2 and by serum- and glucocorticoid-dependent kinase 1. *Am J Physiol Gastrointest Liver Physiol* 287: G143–G150, 2004.
- Palouzier-Paulignan B, Lacroix MC, Aime P, Baly C, Caillol M, Congar P, Julliard AK, Tucker K, Fadool DA.** Olfaction under metabolic influences. *Chem Senses* 37: 769–797, 2012.
- Persaud A, Alberts P, Amsen EM, Xiong X, Wasmuth J, Saadon Z, Fladd C, Parkinson J, Rotin D.** Comparison of substrate specificity of the ubiquitin ligases Nedd4 and Nedd4-2 using proteome arrays. *Mol Syst Biol* 5: 333, 2009.
- Pongs O, Schwarz JR.** Ancillary subunits associated with voltage-dependent K⁺ channels. *Physiol Rev* 90: 755–796, 2010.
- Rickheit G, Wartosch L, Schaffer S, Stobrawa SM, Novarino G, Weinert S, Jentsch TJ.** Role of CIC-5 in renal endocytosis is unique among CIC exchangers and does not require PY-motif-dependent ubiquitylation. *J Biol Chem* 285: 17595–17603, 2010.
- Rotin D, Staub O.** Role of the ubiquitin system in regulating ion transport. *Pflügers Arch* 461: 1–21, 2011.
- Rougier JS, van Bemmelen MX, Bruce MC, Jespersen T, Gavillet B, Apotheloz F, Cordonier S, Staub O, Rotin D, Abriel H.** Molecular determinants of voltage-gated sodium channel regulation by the Nedd4/Nedd4-like proteins. *Am J Physiol Cell Physiol* 288: C692–C701, 2005.
- Sambrook J, Fritsch EF, Maniatis T.** *Molecular Cloning: a Laboratory Manual*. New York: Cold Spring Harbor Laboratory, 1989.
- Steidl JV, Yool AJ.** Differential sensitivity of voltage-gated potassium channels Kv1.5 and Kv12 to acidic pH and molecular identification of pH sensor. *Mol Pharmacol* 55: 812–820, 1999.
- Sudol M, Hunter T.** NeW wrinkles for an old domain. *Cell* 103: 1001–1004, 2000.
- Tan JM, Wong ES, Kirkpatrick DS, Pletnikova O, Ko HS, Tay SP, Ho MW, Troncoso J, Gygi SP, Lee M, Dawson VL, Dawson TM, Lim K.** Lysine 63-linked ubiquitination promotes the formation and autophagic clearance of protein inclusions associated with neurodegenerative diseases. *Hum Mol Genet* 17: 431–439, 2008.
- Thiebaud N, Johnson MC, Butler JL, Bell GA, Ferguson KL, Fadool AR, Fadool JC, Gale AM, Gale DS, Fadool DA.** Hyperlipidemic diet causes loss of olfactory sensory neurons, reduces olfactory discrimination, and disrupts odor-reversal learning. *J Neurosci* 34: 6970–6984, 2014.
- Thiebaud N, Llewellyn-Smith I, Gribble F, Reimann F, Trapp S, Fadool DA.** The incretin hormone glucagon-like peptide 1 increases mitral cell excitability by decreasing conductance of a voltage-dependent potassium channel. *J Physiol* 594: 2607–2628, 2016.
- Tucker K, Cho S, Thiebaud N, Henderson MX, Fadool DA.** Glucose sensitivity of mouse olfactory bulb neurons is conveyed by a voltage-gated potassium channel. *J Physiol* 591: 2541–2561, 2013.
- Tucker K, Fadool DA.** Neurotrophin modulation of voltage-gated potassium channels in rat through TrkB receptors is time and sensory experience dependent. *J Physiol* 542: 413–429, 2002.
- Tucker K, Cavallin M, Overton JM, Fadool DA.** Ion channel in the olfactory bulb subserves as a metabolic sensor (Abstract). *Chem Senses* 35: 638, 2010.
- Tucker K, Overton JM, Fadool Kv1 DA.3.** gene-targeted deletion alters longevity and reduces adiposity by increasing locomotion and metabolism in melanocortin-4 receptor-null mice. *Int J Obes (Lond)* 32: 1222–1232, 2008.
- Tucker K, Overton JM, Fadool DA.** Diet-induced obesity resistance of Kv1.3^{-/-} mice is olfactory bulb dependent. *J Neuroendocrinol* 24: 1087–1095, 2012a.
- Tucker KR, Godbey SJ, Thiebaud N, Fadool DA.** Olfactory ability and object memory in three mouse models of varying body weight, metabolic hormones, and adiposity. *Physiol Behav* 107: 424–432, 2012b.
- Upadhyay SK, Eckel-Mahan KL, Mirbolooki MR, Tjong I, Griffey SM, Schmunk G, Koehne A, Halbout B, Iadonato S, Pedersen B, Borrelli E, Wang PH, Mukherjee J, Sassone-Corsi P, Chandy Selective Kv1 KG.3. channel blocker as therapeutic for obesity and insulin resistance. *Proc Natl Acad Sci USA* 110: E2239–E2248, 2013.**
- Vecchione A, Marchese A, Henry P, Rotin D, Morrione A.** The Grb10/Nedd4 complex regulates ligand-induced ubiquitination and stability of the insulin-like growth factor I receptor. *Mol Cell Biol* 23: 3363–3372, 2003.
- Xu J, Koni PA, Wang P, Li G, Kaczmarek LK, Wu Y, Li Y, Flavell RA, Desir GV.** The voltage-gated potassium channel Kv1.3 regulates energy homeostasis and body weight. *Hum Mol Genet* 12: 551–559, 2003.
- Yang B, Kumar S.** Nedd4 and Nedd4-2: closely related ubiquitin-protein ligases with distinct physiological functions 4. *Cell Death Differ* 17: 68–77, 2010.
- Zeberg H, Blomberg C, Arhem P.** Ion channel density regulates switches between regular and fast spiking in soma but not in axons. *PLoS Comput Biol* 6: e1000753, 2010.